Article

Cell

Independent and Stochastic Action of DNA Polymerases in the Replisome

Graphical Abstract

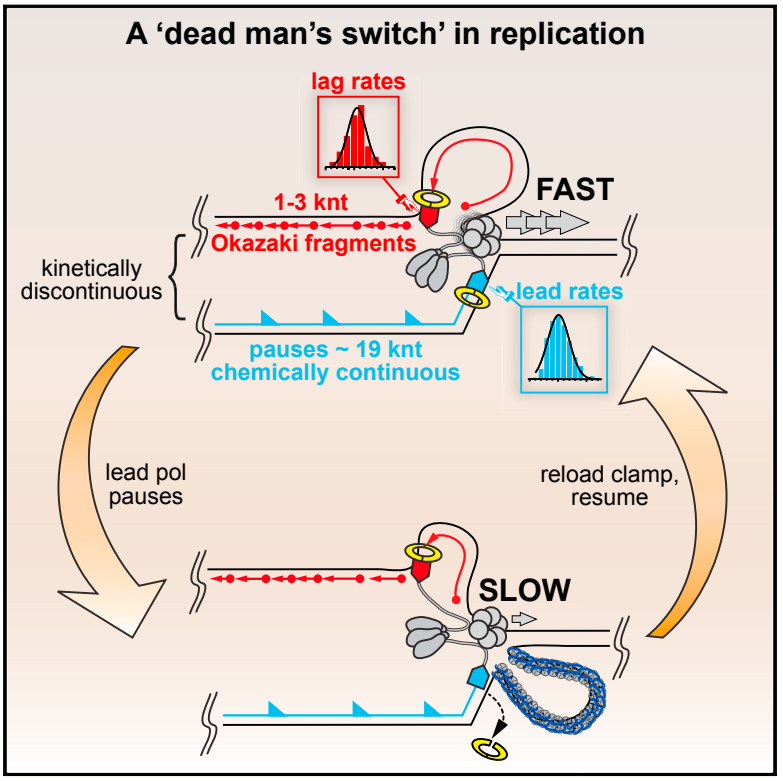

Highlights

- Leading- and lagging-strand polymerases function autonomously within a replisome
- Replication is kinetically discontinuous and punctuated by pauses and rate-switches
- The helicase slows in a self-regulating fail-safe mechanism when synthesis pauses
- Priming is scaled to a 5-fold reduced processivity of the lagging-strand polymerase

Authors

James E. Graham, Kenneth J. Marians, Stephen C. Kowalczykowski

Correspondence

kmarians@sloankettering.edu (K.J.M.), sckowalczykowski@ucdavis.edu (S.C.K.)

In Brief

Polymerases within the replisome operate independently and discontinuously, and they are not coordinated.

Graham et al., 2017, Cell *169*, 1201–1213
June 15, 2017
http://dx.doi.org/10.1016/j.cell.2017.05.041

CellPress

Cell

Independent and Stochastic Action of DNA Polymerases in the Replisome

James E. Graham,[1,3] Kenneth J. Marians,[2,*] and Stephen C. Kowalczykowski[1,4,*]
[1]Department of Microbiology and Molecular Genetics and Department of Molecular and Cellular Biology, University of California, Davis, Davis, CA 95616, USA
[2]Molecular Biology Program, Memorial Sloan Kettering Cancer Center, 1275 York Avenue, New York, NY 10065, USA
[3]Present address: Oxford Nanopore Technologies, Edmund Cartwright House, 4 Robert Robinson Avenue, Oxford Science Park, Oxford OX4 4GA, United Kingdom
[4]Lead Contact
*Correspondence: kmarians@sloankettering.edu (K.J.M.), sckowalczykowski@ucdavis.edu (S.C.K.)
http://dx.doi.org/10.1016/j.cell.2017.05.041

SUMMARY

It has been assumed that DNA synthesis by the leading- and lagging-strand polymerases in the replisome must be coordinated to avoid the formation of significant gaps in the nascent strands. Using real-time single-molecule analysis, we establish that leading- and lagging-strand DNA polymerases function independently within a single replisome. Although average rates of DNA synthesis on leading and lagging strands are similar, individual trajectories of both DNA polymerases display stochastically switchable rates of synthesis interspersed with distinct pauses. DNA unwinding by the replicative helicase may continue during such pauses, but a self-governing mechanism, where helicase speed is reduced by ~80%, permits recoupling of polymerase to helicase. These features imply a more dynamic, kinetically discontinuous replication process, wherein contacts within the replisome are continually broken and reformed. We conclude that the stochastic behavior of replisome components ensures complete DNA duplication without requiring coordination of leading- and lagging-strand synthesis.

INTRODUCTION

The *Escherichia coli* genome is replicated at ~650 bp•s^{-1} in vivo (Pham et al., 2013) by a replisome comprising at least 13 distinct polypeptides. The hexameric helicase DnaB, which translocates 5′→3′ on the lagging-strand template, unwinds DNA at the replication fork. DNA synthesis is catalyzed by two core polymerases (Dohrmann et al., 2016), whose activities are inferred to be coordinated. Core polymerase ($\alpha\varepsilon\theta$) is poorly active and requires the β-clamp ("β"; a dimer of DnaN), topologically linked around DNA, for processive synthesis. The clamp-loader complex ($\tau_2\gamma\delta\delta'\chi\psi$) places β on the 3′ terminus of primer-template junctions. The τ subunit of the clamp loader organizes the helicase, core polymerases, and clamp-loader into a single complex, permitting the rapid and concomitant replication of both parental strands.

DNA must be replicated completely and faithfully so that large ssDNA gaps are not left that might destabilize the genome. Leading- and lagging-strand synthesis proceed in overall opposite net directions. "Okazaki fragments" (OFs), 1–3 kb fragments synthesized discontinuously on the lagging strand, are extended and ligated behind the replisome to yield a continuous duplex (Okazaki et al., 1967). Each OF is initiated by the synthesis of a short RNA primer by primase (DnaG) that is extended by core polymerase complexed with β; β is used stoichiometrically for the synthesis of each OF. Primase thus governs the periodicity of lagging-strand synthesis, with OF length inversely correlated with primase concentration (Wu et al., 1992a). This model suggests that one polymerase replicates each strand exclusively, requiring the lagging-strand polymerase to cycle from one primer to the next upon OF completion. For lagging-strand synthesis to proceed without leaving large gaps, the distance between priming events must therefore be less than the mean polymerase processivity.

One would expect two biochemically identical core polymerases to extend DNA at similar rates. However, it has been proposed that lagging-strand synthesis should be faster overall to accommodate binding of primase to DnaB, synthesis of a primer and dissociation of primase, loading β, binding of β by core polymerase, and primer extension to complete the OF (Georgescu et al., 2014; Pandey et al., 2009; Selick et al., 1987; Wu et al., 1992a). If not, then such slow steps would require a delay of the leading-strand polymerase to accommodate lagging-strand synthesis. Any model of replication must therefore rationalize how the leading-strand polymerase does not advance so far ahead of the lagging-strand polymerase that synthesis by the two polymerases becomes discoordinated (what has been termed "uncoupled") (Yeeles and Marians, 2013). Two independent proposals are that either (1) lagging-strand synthesis or primase itself, directly as a "molecular brake," slows replication (Lee et al., 2006; Yao et al., 2009) or (2) that the rate of helicase unwinding is regulated by the polymerase itself (Stano et al., 2005) should the two become physically separated or functionally "uncoupled."

A commonly held view is that leading-strand synthesis is both continuous and highly processive. However, some evidence suggests a more dynamic scenario (Duderstadt et al., 2016; Geertsema et al., 2014; Langston et al., 2009; Yeeles and

Marians, 2011). The leading-strand polymerase can stall at a lesion, but DNA unwinding continues, and primase re-primes the leading strand downstream of the lesion (Yeeles and Marians, 2011). This mechanism permits rapid lesion bypass without fork disassembly and restart.

The relationship between leading- and lagging-strand synthesis has been determined in bulk by labeling and separating the two daughter strands by alkaline gel electrophoresis, which revealed the roles of proteins and nucleotide concentrations on lagging-strand synthesis (Wu et al., 1992a; 1992b). However, ensemble experiments are limited: (1) long product lengths cannot accurately be measured; (2) without nucleotide bias, leading- and lagging-strand synthesis at limiting primase concentration cannot unequivocally be distinguished; and (3) the ensemble obscures the activity of single molecules, and transient events (e.g., stochastic pauses) cannot be observed.

Here, we observe the behavior of single replisomes actively engaged in DNA replication in real time, using total internal reflected fluorescence (TIRF) microscopy. We show that single replisomes containing two core polymerases in the presence of excess β, single-stranded DNA-binding protein (SSB), and primase are sufficient to fully duplicate up to ~250 kb of DNA. Synthesis by the core polymerases is unexpectedly dynamic, with synthesis interspersed with pauses. Though rates of the leading- and lagging-strand polymerases are similar, the rates of individual polymerases can vary 10-fold and are changeable. Leading-strand synthesis by a single replisome proceeds for ~70 kb on average, whereas lagging-strand synthesis is limited to ~14 kb; curiously, leading-strand synthesis is punctuated by pauses every ~19 kb, perhaps reflecting an intrinsic lifetime of components within the complex that is manifest similarly in lagging-strand processivity and leading-strand pausing. Overall processivity of the replication fork is unaffected by the concentration and activity of primase, showing that leading- and lagging-strand polymerases can function autonomously, and establishing that primase does not regulate polymerization. Furthermore, helicase speed is regulated in a self-governing manner to prevent runaway DNA unwinding: upon polymerase pausing, the helicase reduces its speed by about 80%, but upon resumption of synthesis, unwinding and replication continue at the normal coupled speeds. We present a model in which either of the polymerases within the replisome acts autonomously in time and in a stochastic manner.

RESULTS

Establishment of a Rolling-Circle Replication Assay Capable of Distinguishing between Leading- and Lagging-Strand Synthesis

To determine rates of leading- and lagging-strand synthesis, priming, and DNA unwinding during replication, we devised a rolling-circle assay that is capable of visualizing replication of both strands, and we observed the products by single-molecule TIRF microscopy (Figures 1A–1C). The rolling-circle assay permits continuous monitoring of DNA replication, so processivity measurements are not limited by template length (Alberts et al., 1983; Pomerantz et al., 2008; Tanner et al., 2009; Yao et al., 2009). We used an 8.6 kb template that could be resolved from the long, duplex tail of the product based on its size and brightness. A reaction comprising all replisome components is shown (Figures 1D–1F). The template, bearing a 5′ biotin tail, was adsorbed onto a coverglass via biotin-streptavidin interaction (Figures 1B and 1C). DnaB, DnaC810, Pol III* [$(\alpha\varepsilon\theta)_2\tau_2\gamma\delta\delta'\chi\psi$], β, three of the four dNTPs, and all four rNTPs were added to the flow-cell, forming an idling, ''pre-initiation'' complex (Figure 1C) in which only the leading-strand polymerase is engaged with β. DnaC810 is a gain-of-function mutant that bypasses the requirement of PriA for loading DnaB (Xu and Marians, 2000) and was used to load DnaB on the template. Excess DnaB, DnaC810, and Pol III* were washed out, and replication was initiated by introducing primase, β, and SSB in the presence of all four dNTPs and rNTPs. The replication reactions were therefore single-turnover with respect to replisomes. On average, ~18% of the template molecules initiated replication during live observations (*N* [replicates] = 3; *n* [molecules] = 650), although the amount varied from 12%–26%. Replication products were visualized in real time by extension under flow in the presence of SYTOX Orange, which detects dsDNA, but not ssDNA•SSB. Figure 1D and Movie S1 show a representative field in which many circular template molecules—small foci at the start of reaction—are replicated to yield long products. The template, at the head of the fork, tracks from left to right in the direction of flow. All products in this field consisted almost entirely of duplex DNA, confirming coordinated leading- and lagging-strand synthesis. Three actively extending molecules are identified in Figure 1D. Frames from videos of each molecule and kymographs (Figures 1E and 1F) show that the average rate of fork movement was largely monotonic, although the fine structure in the trajectories will be addressed below. By tracking the position of the circle with respect to its anchor position, we determined the length of the replication product as a function of time (Figure 1F, magenta, cyan, and green traces). DNA products could be ~250 kb in length (Table 1); linear fits to the full trajectories (n = 84) yielded a Gaussian distribution of rates with a mean of 470 ± 180 bp•s^{-1} (± SD) (Figures 1F and 1G).

Primase Is the Only Replication Protein Specific to Lagging-Strand Synthesis

We next considered which proteins are specific to lagging-strand synthesis. We initially analyzed the end products of replication by performing the reactions as above, omitting key replication proteins in turn without laser illumination under low flow (Figures S1A–S1D) to reduce the force on the replisome yet replenish proteins and nucleotides. Reactions were quenched after 10 min, and products were extended for length measurement under high flow and laser illumination (Table 1 and STAR Methods).

When all proteins were present, the median product length was 68 kb after 10 min, and virtually all product was duplex (Figure 2A). However, for some protein dropouts, replication products were short, and when imaged under flow, they appeared as small foci that were nearly indistinguishable from unreacted template (e.g., primase omitted, Figure 2A, vi). We used a flow-cycling method to determine where the products were anchored (Figure S2 and STAR Methods); anchor positions are shown via a composite image showing the same fields with flow turned off in cyan and flow-extended molecules in magenta (Figure 2A, ii, iii,

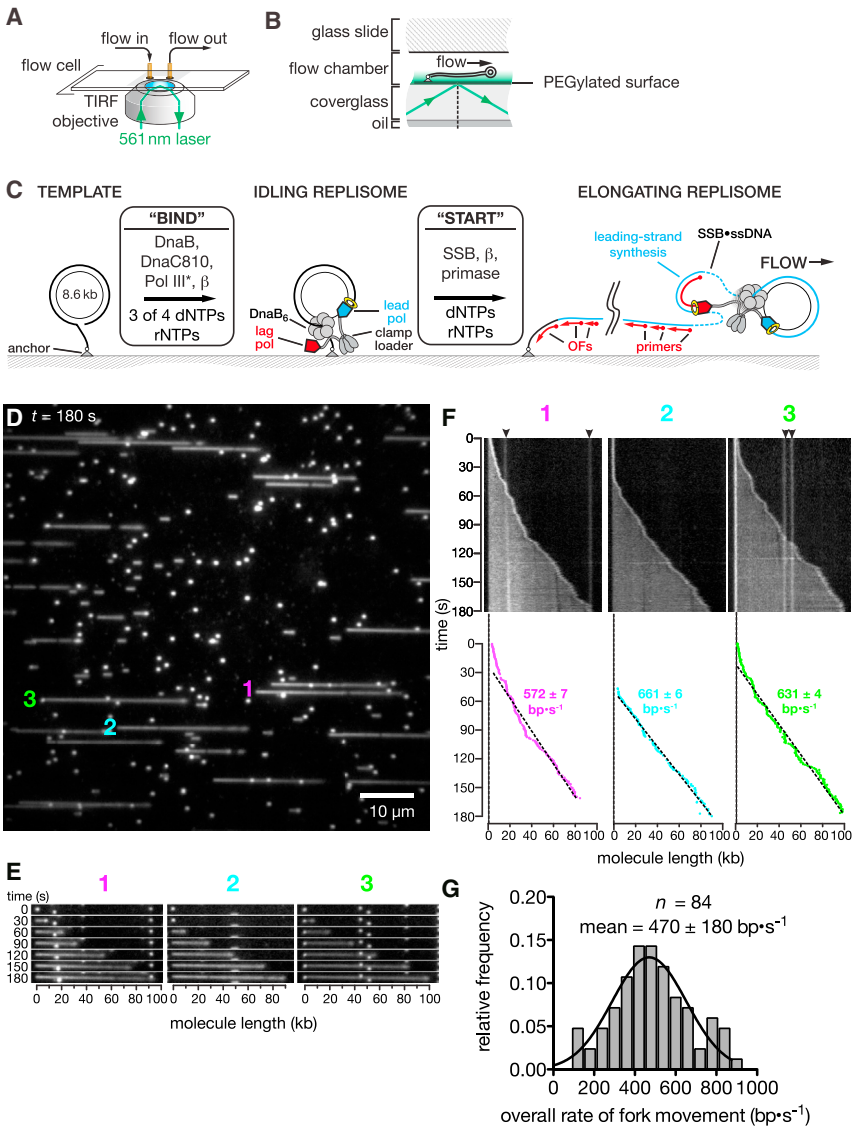

Figure 1. Visualizing Leading- and Lagging-Strand Synthesis Using a Rolling-Circle Single-Molecule Assay

(A) Schematic of TIRF microscope and flow-channel.

(B) Side-on view, showing surface-attached DNA replication products.

(C) Cartoon showing assembly and live visualization of replication. dsDNA is visualized with SYTOX Orange fluorescent stain.

(D) Micrograph showing products live, ~180 s from start; three extending molecules identified. Scale bar, 10 μm, equal to 37.0 kb dsDNA at 2,500 μl/hr (Figure S1).

(E) Time-lapse of three replicating molecules from (D), showing synthesis with time.

(F) Kymographs of molecules from (D), showing linear fits to trajectories yielding average rates of replication fork progression. Arrowheads: non-replicating substrates.

(G) Histogram of replication rates; mean rate, 470 ± 180 bp•s^{-1} (molecules, n = 84) from Gaussian fit.

iv, and vi). The lengths of replication products confirmed the canonical roles for each protein (Wu et al., 1992a) (Table 1). DNA synthesis was dependent on both DNA unwinding by DnaB (Figure 2A, ii) and synthesis by Pol III* (Figure 2A, iii).

The three proteins that act distributively—β, SSB, and primase—affected synthesis in different ways (Figure 2A, iv–vi). Omission of β did not affect the nascent lagging strand specifically, yielding duplex products; however, products were short, showing β's essential role in increasing the processivity of synthesis by core polymerase on both strands, and the length of extended products was reduced by 79% to 14 kb (Figure 2A, iv; Table 1). Omitting SSB reduced the median product length to ~29 kb, suggesting that SSB stimulates DNA synthesis on both leading and lagging strands, as has been suggested previously (Georgescu et al., 2014) (Figure 2A, v; Table 1).

Only primase affected lagging-strand synthesis specifically (Figure 2A, vi), as expected from ensemble experiments (Mok and Marians, 1987; Wu et al., 1992a). Products generated without primase consisted of a template anchored via long tails of ssDNA•SSB to the surface (Figure 2B). We determined the lengths of the SSB-ssDNA products produced by replication of only the leading strand, using the calibrations in Figures S1E–S1H and the method of Figure S2. Omitting primase did not significantly affect the median product length (~77 knt), although the product was fully ssDNA (Table 1). Thus, leading-strand synthesis occurs independently of lagging-strand synthesis.

We expected that, because product lengths were similar in the presence and absence of primase, the rate of leading-strand replication would also be independent of primase. We therefore monitored replication in real time under extension (Figure 2B). In these reactions, only leading-strand ssDNA•SSB is produced, so SYTOX Orange stains only the rolling-circle template, which moves across the field in the direction of flow. Figures 2C and 2D and Movie S2 show a composite of video frames at 50 s intervals; three representative molecules are identified. By tracking the position of each template molecule, we determined product lengths as a function of time. Figure 2E shows kymographs derived from the three molecules identified in Figure 2C and linear fits to the data to yield rates of leading-strand synthesis. Overall rates of extension were approximately linear, as per the reaction containing primase, but were interspersed with occasional pauses and termination events (Figure 2E). The mean rate of fork progression, from initiation to termination, including pauses, was 390 ± 130 nt•s^{-1}. Notably, this rate is not significantly different from the replication speed in the presence of primase, 470 ± 180 nt•s^{-1} (Figure 2F), and the transient pauses are

Table 1. Size Distribution of Products from Complete Replication Reaction and when Protein Components Omitted

	OBSERVED PRODUCT LENGTH		SUBSTRATE UTILIZATION	
protein(s) omitted	median total length of molecule [interquartile range, maximum]	*n*	extended product (%)	*n*
none	68 kb [35-110, **246**]	1,047	28	427
DnaB, DnaC810	0[a]	62[a]	0	440
Pol III*	0[a]	28[a]	0	128
β	14 kb [10-17, **43.6**]	66	4	574
SSB	28.8 kb [17.9-49.5, **121**]	116	7	285
primase	77 knt [50.1-118, **238**]	138	44	159

Median product lengths (total length of leading strand, measured from anchor to template) ± interquartile range; *n*, number of molecules observed.
[a], no extended products observed.

independent of primase. Thus, we find no evidence for the *E. coli* replisome that primase acts as a molecular brake to regulate synthesis of the leading-strand DNA polymerase, in agreement with an alternative analysis of the T7 replication system (Pandey et al., 2009).

We measured the processivities of replisomes from the real-time imaging experiments of Figures 1D and 2C, judged by the final lengths of all molecules in a given field after ~5 min reaction. There was no significant difference between the processivity distributions with or without primase included in the flow (median [interquartile range (IQR)]): 97 [62–110] kb, n = 69; and 88 [62–118] knt, n = 49; Figure 2G). Processivity was markedly reduced by the absence of β in the flow (median [IQR]: 21 [7–50] kb, n = 62), but there was again no significant difference whether primase was also present in the flow (without primase, median 37 [16–60] knt, n = 53) (Figure 2G). Thus, we find no evidence that priming the lagging strand affects the speed or the processivity of the replisome; however, curiously, the continued presence of β is required to maintain leading-strand synthesis.

The Leading-Strand Polymerase Pauses Stochastically, yet the Helicase Continues Unwinding DNA, albeit More Slowly

The observation of pauses in overall fork progression (Figure 1F) and leading-strand replication (Figure 2E) led us to further investigate their mechanism. We focused first on leading-strand replication only because deconvolution of the data was straightforward and, as shown in Figure 2 and below, leading-strand synthesis was independent of primase. However, as described below, similar pausing behavior was observed for the lagging-strand polymerase.

Leading-strand polymerases were seen to stochastically pause once, several times, or not at all (Figure 3A). By fitting the trajectories to multi-segment lines, we determined the pause duration, the amount of DNA synthesized during each burst, and the "burst" rates for synthesis between pauses. Fits for three representative molecules (molecules a, b, and c, Figures 2C and 3A, i), with kymographs derived from the raw data (Figure 3A, ii) are shown together with an expanded movie of the same three molecules (Movie S3). The trajectories show that an individual DNA polymerase pauses randomly and then resumes synthesis, although at a different rate; detailed analysis follows.

Next, we considered whether DnaB continues to unwind the dsDNA ahead of the polymerase during a pause. Unwinding without synthesis would reduce the fluorescent signal; if synthesis did not restart, DnaB would run off the end of the template, and replication would terminate (Figure S3A). To reveal unwinding events, we measured the intensity of the template over time, at the position of the pause, and normalized the maximum intensity observed to intact template (~8.6 kb) to estimate the duplex content of the template during replication. The intensity traces exhibited a characteristic sawtooth pattern: a slow monotonic decrease in fluorescence, often followed by a fast increase back to the full template intensity (Figure 3A). Overlaying the unwinding and synthesis trajectories revealed that the unwinding portion of these patterns initiated upon pausing of leading-strand synthesis in 90% of cases (62 events). Terminal unwinding events were also observed as leading-strand synthesis ceased, which we interpret as DnaB runoff (Figure 3A; Movie S3, molecules a and c). Remarkably, the recovery of fluorescence following the slow decrease occurred in 65% of unwinding events during elongation (40/62 events; 67 molecules), e.g., Figure 3, molecule b at ~320 s. We interpret this as resumption of fast, leading-strand synthesis following a pause. Pausing was unaffected by increasing SSB concentration or flow (Figures S3B and S3C). Thus, the helicase and leading-strand polymerase can become transiently unsynchronized: unwinding can continue without synthesis, albeit at a reduced rate. Nevertheless, as we discuss below, this observation does not necessarily imply that the two become physically disengaged.

We hypothesized that pauses in leading-strand synthesis might be caused by polymerase dissociation either from DNA or β or from stalling. Pauses might be intrinsic to polymerization, or they might be caused by DNA damage or difficult-to-replicate secondary structure. If the polymerase were to dissociate from DNA or β during a pause, resumption of synthesis would presumably require reloading of β at the 3′ terminus of the leading strand. We therefore compared the trajectories of leading-strand-only replication in the presence and absence of β in the flow (Figures 3B–3E and S3D and Movie S4). We discovered that omission of β changed the burst rates (the rates of elongation between detectable pauses) of leading-strand synthesis. Figure 3B shows the rate distribution for bursts of leading-strand synthesis. With β present, the distribution is well described by a single Gaussian, with a mean of 510 ± 190 nt•s^{-1} (± SD; median, 520 nt•s^{-1}); however, with β absent from flow, we observed an additional, slower population of molecules with a mean of 270 ± 90 nt•s^{-1}, in addition to the fast population of 560 ± 120 nt•s^{-1} (overall median, 450 nt•s^{-1}). Note that for both distributions, the width of each Gaussian is much larger than the precision of an individual rate measurement (e.g., in Figure 3A, the SD for defining an individual trajectory ranges from ± 3 to ± 29 nt•s^{-1}), revealing intrinsic heterogeneity in the synthesis behavior of individual polymerases.

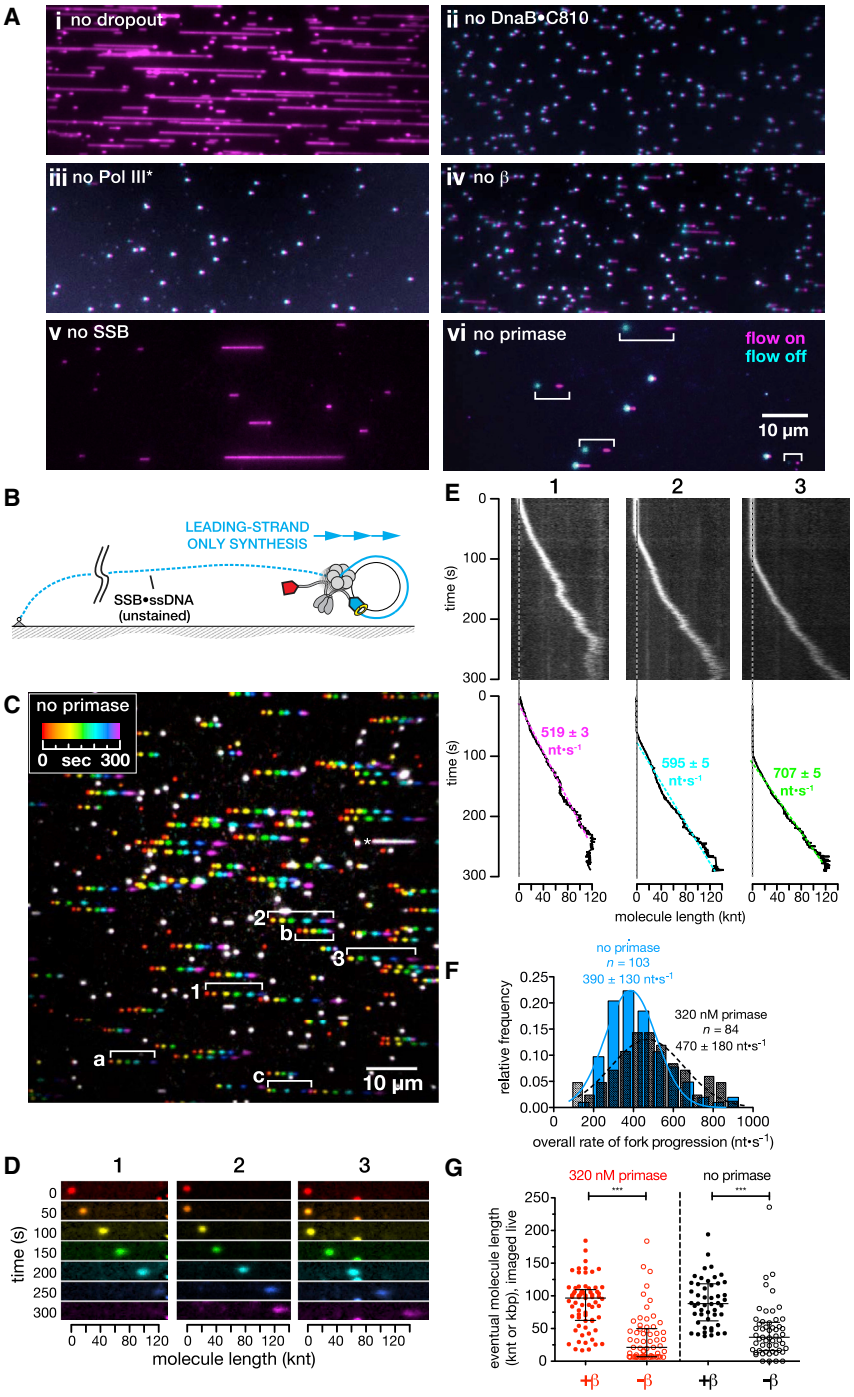

Figure 2. Individual Replication Fork Progression Is Independent of Primase

(A) Micrographs showing replication products at 10 min where (i) all components present, or a component omitted; (ii) DnaB and DnaC810; (iii) Pol III*; (iv) β; (v) SSB; (vi), primase. Composite, false-colored fields show anchor points for molecules that contain ssDNA, except i or v, where only long products were seen. In vi, surfaces were sparsely populated with DNA to avoid any ambiguity in molecule identification. Cyan, fields with flow off; magenta, same field with flow on, showing fully extended molecules. Molecules are bracketed for clarity. Scale bar, 10 μm, equal to 33.9 kb dsDNA or 80.3 knt SSB-bound ssDNA at 4,000 μl/hr, without Mg^{2+} under end-point conditions (Figure S1).

(B) Cartoon showing leading-strand-only product in a reaction lacking primase.

(C) Composite, false-colored image showing leading-strand-only replication without primase. Three replicating molecules (1, 2, 3) are identified with brackets. Image shows motion of the SYTOX Orange-stained circular template across the field. The field is composed of seven snapshots at 50 s intervals, colored red through violet (see legend). Scale bar, 10 μm, equal to 105 knt ssDNA•SSB at 2,500 μl/hr under live conditions (Figure S1). Asterisk (*) denotes spurious priming event (see also Movie S2). Molecules a, b, and c are referred to later.

(D) Time-lapse, at 50 s intervals, of molecules 1, 2, and 3 identified in (C), colored by time-point as per (C).

(E) Kymographs of molecules, numbered per (C) and (D), showing fork progression without primase. Dashed gray line: position of anchor. Linear fits are from initiation to termination, yielding average fork rates. Pauses are included in the average here.

(F) Histograms of fork progression rates in the presence (gray) and absence of primase (light blue). Histograms fit to single Gaussians (R^2: with primase, 0.80; without primase, 0.94); no outliers were rejected. *n*, molecules.

(G) Processivities of single replisomes from live-imaging experiments. Whisker plots of molecule lengths, with (320 nM) or without primase, and either with or without β in flow. Data from two (primase, no β) or three (others) experiments. Horizontal bars, median; vertical bars, interquartile range. Three asterisks (***) denote significantly different pairs of populations (Kruskal-Wallis; $p < 0.05$); other pairs not significantly different.

Furthermore, after pausing, the rate of synthesis typically changed, revealing stochastic switching.

Differences in the median burst length (19 knt versus 9.7 knt without β) show that the polymerase manifests an increased propensity to pause in the absence of free β (Figure 3C). Pause durations are exponentially distributed, and half-times increased slightly in the absence of free β from ~12 s to ~18 s, although within the range of errors (Figure 3D). Thus, pausing is more frequent in the absence of β and is associated with a sub-population of polymerases with a reduced synthesis rate, suggesting that loss of the interaction between core polymerase and β during replication is responsible. Thus, a portion of the leading-strand pauses in synthesis may occur via a mechanism that requires reloading β for resumption.

We wondered whether the dsDNA unwinding rate by DnaB would be affected by polymerase pausing. We therefore analyzed unwinding events observed during elongation pauses from experiments with and without β in flow. Markedly similar distributions

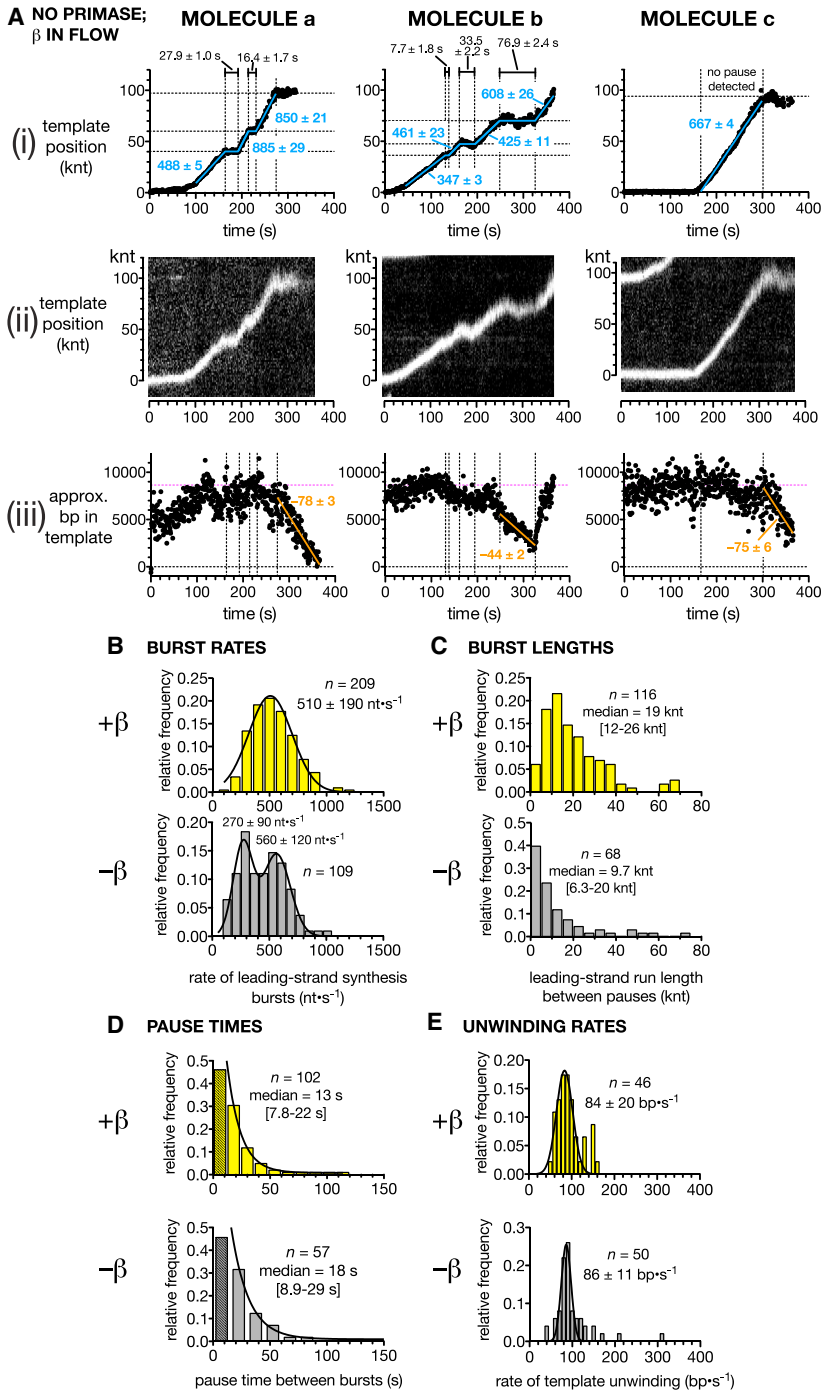

Figure 3. Leading-Strand Polymerization Is Kinetically Discontinuous

(A) Correlation of leading-strand-only synthesis pauses with duplex unwinding. (i) Plots of template displacement against time for molecules a, b, and c (Figure 2C) replicating without primase. Data were fit to segment lines (blue lines), yielding rates of synthesis (nt•s^{-1}), pause times and positions, and the lengths of synthesis bursts between pauses. (ii) Kymographs of the molecules in (i). (iii) Determination of DNA unwinding rates during pauses in synthesis. Sections of monotonic unwinding fit with straight lines (orange; rates in bp•s^{-1}), using pauses (i) as points of inflection. Magenta dotted lines: fully base-paired template (8,644 bp).

(B–E) Histograms of (B) burst rates of leading-strand synthesis, (C) run lengths of bursts between pauses, (D) pause times between bursts, and (E) DNA unwinding rates, determined without primase and in the presence (yellow) or absence (gray) of β. Data from five (+β) or three (−β) experiments and *n* observations. Means from single- or double-Gaussian fits ± SD (R^2: [B], +β, 0.97; −β, 0.97; [E], +β, 0.97, excluding outliers > 130 bp•s^{-1}; −β, 0.87). Data in (D) fit to single exponential (+β, τ ~12 s, R^2 = 0.99; −β, τ ~15 s; R^2 = 0.96), ignoring the under-sampled first bin. *n*, trajectories = 100.

of DNA unwinding velocities (84 ± 20 with, 86 ± 11 bp•s^{-1} without, free β; Figure 3E), identical to single-molecule results using magnetic tweezers (~80 bp•s^{-1} at zero force [Ribeck et al., 2010]), were observed. However, these velocities are ~one-sixth the burst velocity of the elongating leading-strand polymerase, and ~one-fifth the overall velocity of the fork. Thus, we directly demonstrate cooperation between leading-strand synthesis and duplex unwinding: DNA polymerase stimulates the activity of DnaB helicase. This cooperativity ensures that runaway unwinding is disfavored when DNA synthesis is paused.

Neither Priming Frequency nor Okazaki Fragment Synthesis Affects Leading-Strand Synthesis

We have shown that the rate and processivity of replisome movement are similar in the presence and absence of lagging-strand synthesis and that most replication forks, under our single-turnover conditions, terminate synthesis after ~5 min replication. However, given the inverse relationship between OF length and primase concentration (Wu et al., 1992a; 1992b), it remained possible that, when priming is infrequent, replication might be delayed by the completion of very long OFs. Therefore, we analyzed replication over a full range of primase concentrations, from none to saturating (320 nM), in the flow along with SSB and β. To collect large datasets spanning multiple fields and eliminate photocleavage during the reaction, we performed experiments under low flow without laser illumination, per Figures 2A–2F, quenching the reactions after 10 min (Figure 4A). The lengths of dsDNA tracts and ssDNA•SSB tracts between duplex tracts were measured under full extension (STAR Methods), subjecting products containing ssDNA at their anchor point to the flow-cycling analysis, per Figures 4A, S2, and S4B.

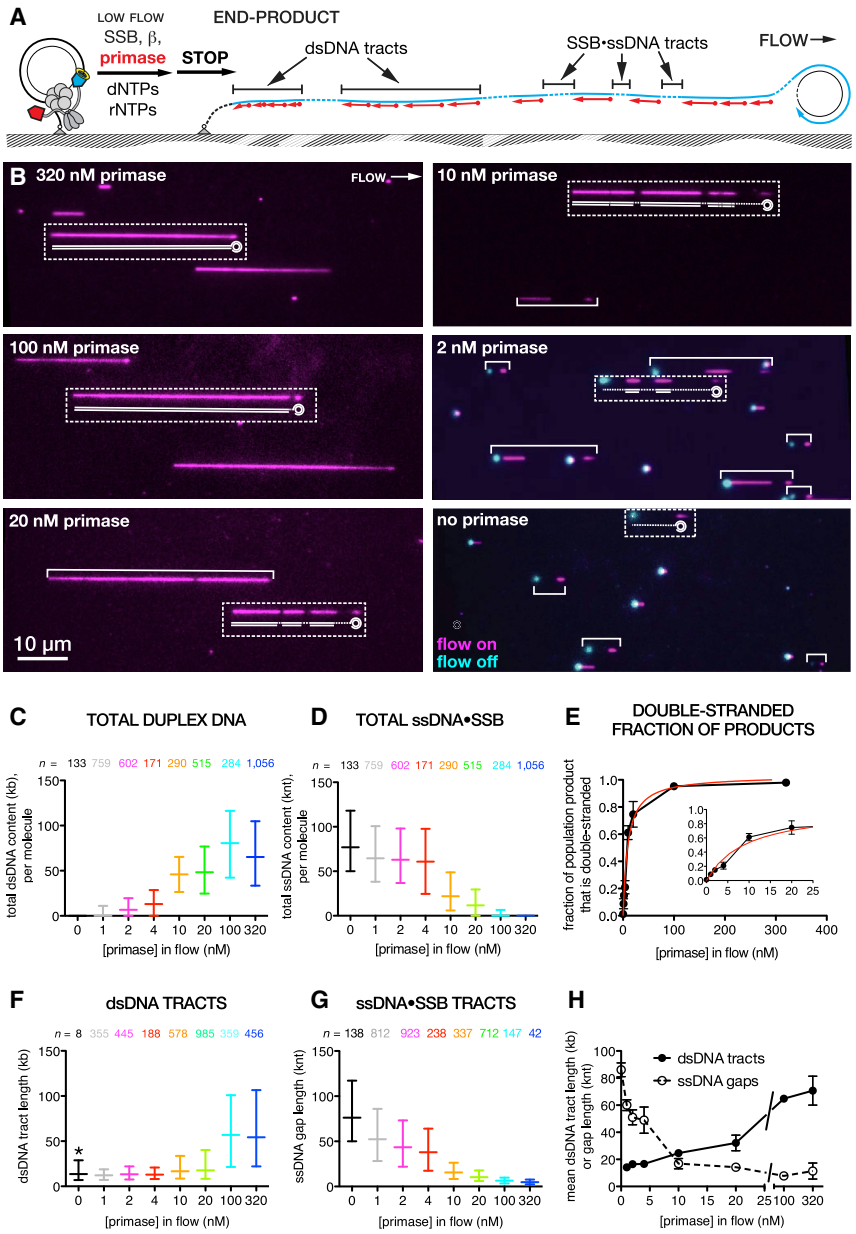

Figure 4. Leading- and Lagging-Strand Polymerases Function Autonomously

(A) Reaction schematic, with experiments performed under low flow and products examined under high flow at a defined end point.

(B) Micrographs of flow-extended products: dsDNA stained by SYTOX Orange; black gaps are ssDNA•SSB. Micrographs are false-colored magenta or cyan to indicate whether flow was pulsed on or off (no primase and 2 nM primase), respectively; molecules are bracketed for clarity. Cartoons (white) show interpretations of dsDNA and ssDNA•SSB tracts for one molecule per panel.

(C and D) Plots of median (horizontal bars) and interquartile range (vertical bars) of (C) total dsDNA and (D) total ssDNA•SSB per molecule for range of primase concentrations ($\geq$ 3 replicates). *n*, total number of molecules.

(E) Plot of fraction of total lagging-strand synthesis per total leading-strand synthesis versus primase concentration; insert shows zoom (replicates, N $\geq$ 3). Data fit to a rectangular hyperbola: $K_{1/2}$ = 9.3 ± 0.9 nM (SE).

(F and G) Plots of median (horizontal bars) and interquartile range (vertical bars) of (F) individual dsDNA tract lengths and (G) individual ssDNA•SSB lengths from N $\geq$ 3 replicates, for range of primase concentrations. *n*, number of molecules observed per condition. Asterisk (*) denotes rare spurious priming events observed at 0 nM primase (n = 8).

(H) Plot of dsDNA and ssDNA•SSB tract lengths versus primase concentration, expressed as the mean of population means (replicates, N $\geq$ 3, ± SEM).

As primase concentration was reduced from 320 nM to zero, the duplex content of replication products decreased, but ssDNA•SSB tract length correspondingly increased (Figures 4B–4D), with half-saturation occurring at 9.3 ± 1.0 nM (± SE) primase (Figure 4E). We also observed an inverse relationship between the mean lengths of individual dsDNA and ssDNA•SSB tracts (Figures 4F–4H), which we treat in detail below. Nevertheless, both the mean total leading-strand length (the sum of dsDNA and ssDNA•SSB in each product) and length distributions both remained virtually unchanged with respect to primase concentration (Figures S4C and S4D). Thus, the progression of replication forks was unaffected by the amount of priming and lagging-strand synthesis. To determine whether primase itself might affect replication in the absence of priming, catalytic site mutants (at 320 nM in flow) were tested: D269A, retaining ~3% activity, showed infrequent priming; and D269Q, which showed negligible priming activity (Corn et al., 2005; Rymer, 2012). However, again, the mean leading-strand length remained unchanged (Figure S4E). Thus, combined with our measurements of fork progression in the presence and absence of primase (Figure 2F), we find no evidence that lagging-strand synthesis slows replication.

Direct Labeling of Okazaki Fragments Reveals Priming Frequency

In the above experiments, one dsDNA tract might consist of several OFs with unresolvable gaps between. We thus determined the locations and size distributions of Okazaki fragments in replication end-products (Figure 5A). We pulse-labeled 3′ OF termini after 10 min of replication with digoxigenin-dUTP, imaging the 3′ termini with fluorescent α-digoxigenin (STAR Methods and Table S1). We define priming distance (PD) as the distance between successive primers (i.e., between 5′ ends of successive OFs). Composite, false-colored fields

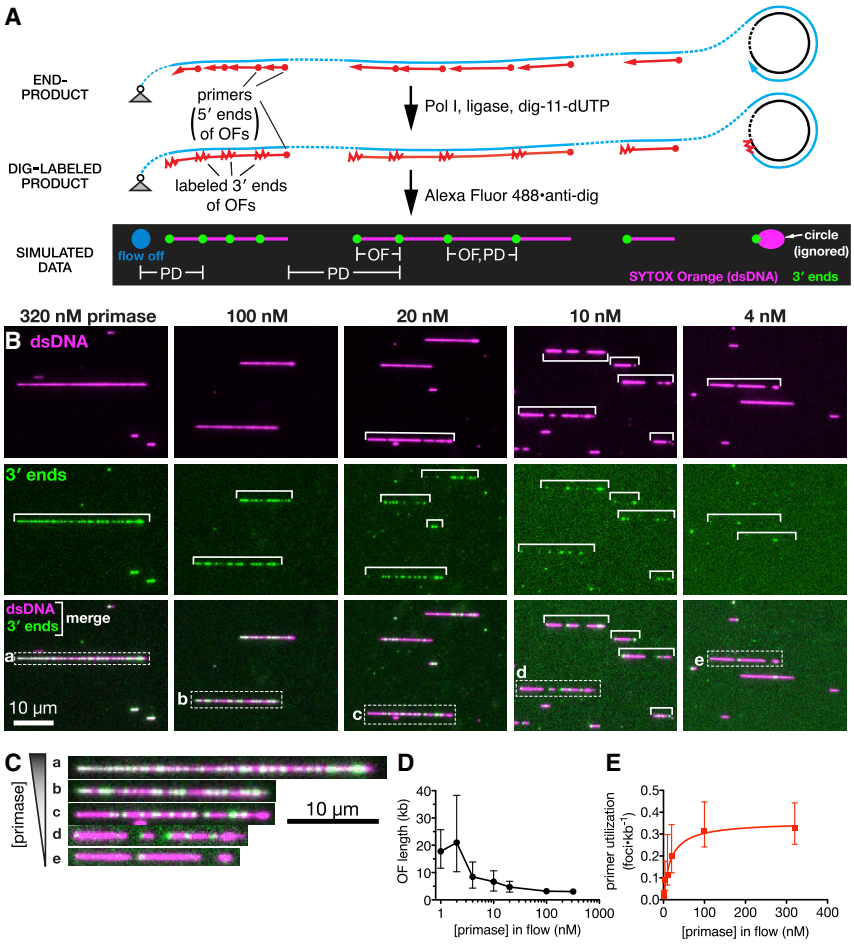

Figure 5. Visualization of Okazaki Fragment Termini Shows a Direct Relationship between Primase Concentration and Priming Frequency

(A) Cartoon (top) showing method used to label 3′ ends of OFs ends (red wavy lines; middle). Cartoon (bottom) shows expected product when stained with SYTOX Orange and labeled with anti-digoxigenin (Figure S5): magenta, dsDNA tracts; green, OF 3′ termini; blue, anchor points; OF, Okazaki fragment length; PD, priming distance, which is defined in the text.

(B) Representative false-colored micrographs with 4–320 nM primase in flow. dsDNA (magenta), OF ends (green), and merged images are shown for each field. Molecules are bracketed for clarity. One molecule in each field is highlighted and expanded in (C).

(C) Five magnified molecules from (B), labeled a–e.

(D) Semi-log plot of Okazaki fragment length against primase concentration. Population means ± 95% confidence intervals (bars); replicates, N = 1 for ≥ 2 nM primase); N = 2 for 1 nM primase.

(E) Primer utilization (reciprocal of priming distance) plotted against primase concentration. Data fit to rectangular hyperbola: $K_{M,app}$ = 17 ± 3 nM (SE). Error bars: reciprocal of interquartile range of priming distance.

showing the patterns of dsDNA and 3′ OF terminus staining are shown (Figures 5B and S5; expanded view of five molecules shown in Figure 5C). In these fields, OFs are closely spaced at high primase concentration but become sparser as primase concentration is reduced; gaps between OFs can still be resolved at limiting and intermediate primase concentration.

Figure 5D shows that OF length varied between 3.0 kb (range: 1.0–8.1 kb) at 320 nM primase and ~19 kb (range: 1.8–80 kb) at 1–2 nM primase. The upper plateau value thus reflects the processivity of lagging-strand synthesis. We represent the activity of primase in terms of primer utilization: the frequency of primer synthesis (the reciprocal of PD), normalized to unit length. A plot of primer utilization against primase concentration was hyperbolic (Figure 5E); a Michaelis-Menten fit returns a K_M of 17 ± 3 nM (SE) with no evidence for cooperativity. Assuming the number of primers utilized is proportional to the number synthesized, this value directly reports the affinity of primase for the replisome. Our K_M value is considerably lower than the previously reported K_d of ~1–3 μM between DnaB and DnaG in isolation (Oakley et al., 2005); our figure may reflect the stabilizing effect of additional protein-protein and protein-DNA contacts present in an actively elongating replisome.

The Median Processivity of Lagging-Strand Synthesis Is ~14 kb

The labeling experiments also revealed that each tract consists of, on average, one OF at 1–2 nM primase (Figures 6A and 6B), whereas > 50% of tracts contained two or more OFs at ≥ 4 nM primase. If each tract contained only one OF, then we can assume that lagging-strand synthesis terminated owing to the inherent processivity of the polymerase, rather than any other event such as either collision with or sensing of the downstream primer. We therefore pooled all dsDNA tract lengths from end-point experiments conducted at 1–2 nM primase (from Figure 4), rejecting OFs abutting the anchor point. The median length was 13.6 kb (n = 422; Figure 6C). We also report the median OF length from the OF labeling experiments above at 1–2 nM primase (Figure S6A), which are in close agreement, at 17.8 kb (n = 62). These figures are remarkably similar to the burst distances between pauses on the leading strand measured from the live-imaging experiments lacking primase (Figure 3C; median, 19 knt). Thus, we speculate that leading- and lagging-strand polymerases are biochemically equivalent, although the different interactions with components of the replisome confer distinct phenomenological differences on each polymerase.

Real-Time Observation of Okazaki Fragment Synthesis Reveals that Leading- and Lagging-Strand Polymerases Have Similar Biochemical Properties

The identification of long OFs led us to investigate replication in real time at limiting primase concentration. Figures 6D–6G and Movie S5 show rolling-circle replication with 1 nM primase,

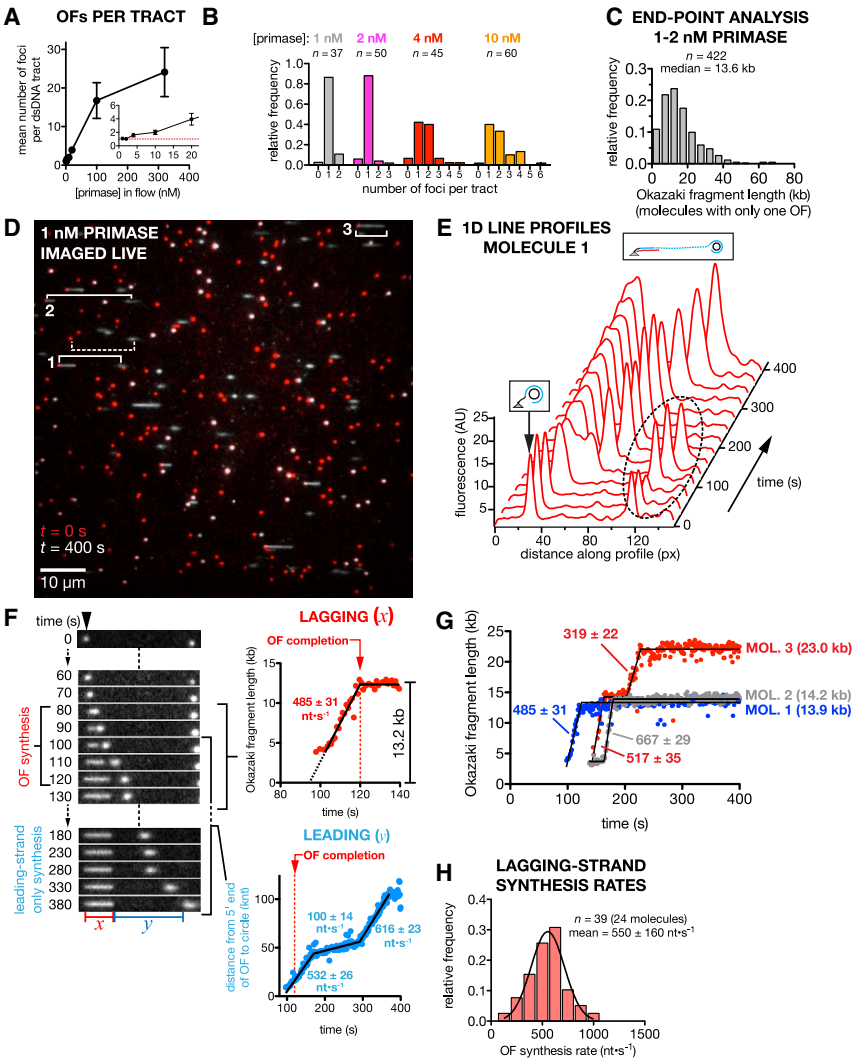

Figure 6. Lagging-Strand Synthesis Occurs at the Same Burst Rate and Processivity as Leading-Strand Synthesis

(A) Plot of mean number (± 95% confidence interval [CI]) of digoxigenin-labeled 3′ foci detected per dsDNA tract (Figure 5) versus primase concentration. Inset: expanded view, showing limit at unity (dashed red line).

(B) Histograms of the number of digoxigenin-labeled 3′ foci detected, as a function of primase concentration. *n*, number of molecules.

(C) Histogram showing distribution of Okazaki fragment lengths from end-product data at 1 nM and 2 nM (replicates, N = 3 per condition; n = 422), assuming one OF per tract. OFs synthesized up to the anchor point were rejected (see text). Only molecules with one OF were considered.

(D) Live replication experiment with 1 nM primase in flow. Image is a false-colored composite of the same field under flow at 0 s (red) and 400 s (grayscale). Three molecules undergoing OF synthesis identified with solid brackets. A molecule that undergoes only leading-strand synthesis is identified with a dotted bracket.

(E) Waterfall plot showing change in fluorescence along a 1D line profile drawn across molecule 1 in (D) over 400 s. Cartoons show interpretation. Dotted ellipse shows a second molecule ignored for the analysis of molecule 1.

(F) Time-lapse of molecule 1 from (D), showing Okazaki fragment synthesis (*x*) and leading-strand-only synthesis (*y*). Graphs (right) show the growth of the OF (top, red, *x*) and leading strand synthesis (bottom, blue, *y*). Data were fit to multiple segmented lines to determine rates (± SE of fit).

(G) Graph showing synthesis of Okazaki fragments for the three molecules in (D). Data fit to segmented lines, with both pauses and end points constrained to zero rate, yielding indicated rates (± SE of fit).

(H) Histogram of lagging-strand burst rates (between pauses) from n = 39 (five experiments; 24 molecules), fit to a single Gaussian to determine population mean ± SD.

β, and SSB in flow, similar to Figures 1D and 2C. Figure 6D shows a representative field, false-colored with the starting material in red and the same field at 400 s in grayscale. Most template molecules were elongated by leading-strand synthesis only. However, duplex DNA appeared behind the template on 36 molecules (N = 5), showing priming and OF synthesis in the expected net 5′–3′ direction toward the anchor-point. Of the 36 lagging-strand synthesis events, 30 (83%) emerged directly (≤ 2 pixels; ~3.6 knt ssDNA•SSB) behind the template, showing that the lagging-strand polymerase is initially associated with the replisome. The median lagging-strand length was 23 kb (n = 20; range 10–57 kb; Figure S6B). Thus, the processivity of Okazaki fragment synthesis observed live approximates that of the equivalent end-point determinations, though over a much smaller sample size. Despite all lagging-strand events initiating at the fork, the lagging-strand polymerase is eventually located several microns from the fork. We suspect that this separation results from spontaneous dissociation, with rebinding prevented by flow and the lagging-strand polymerase either remaining associated with the replisome or the Okazaki fragment. In end-point experiments where the sample size is higher (Figure 6C), 88 molecules (~15%) show more than one Okazaki fragment, demonstrating that the lagging-strand polymerase usually remains as a component of the replisome.

By monitoring the fluorescence profile of lagging-strand synthesis with time (Figure 6E), we could deduce the rate of leading- and lagging-strand synthesis simultaneously. Figure 6E shows the 1D fluorescence line profile of a representative molecule (molecule 1, Figure 6D); initially, the molecule exhibits only leading-strand synthesis, but ~80 s after initiation, a fluorescent tract resulting from OF synthesis appears behind the template and elongates over the next ~40 s. Figure 6F shows individual video frames and Figure S6C shows a kymograph of the same molecule during OF synthesis (from ~80 to 120 s; 10 s steps) and also leading-strand-only synthesis after OF completion (from ~120 s; 40 s steps). Figure 6F shows that the linear extension of the OF in molecule 1 with time occurs at a rate of 485 ± 31 nt•s^{-1}; the 13.2 kb OF is completed at ~120 s because the

lagging-strand polymerase runs into the anchor (Figure S6D, i); leading-strand synthesis continues simultaneously during this period at 532 ± 26 nt•s^{-1} (Figure 6F, lower right). Thus, we observe similar rates of synthesis on both the leading and lagging strands by the same replisome.

Replication also displayed some of the characteristics determined above for leading-strand synthesis where leading-strand polymerases paused, and template molecules occasionally unwound during leading-strand pausing (Figure S6D, iii). Figure 6G shows the trajectories of Okazaki fragment synthesis for the three molecules identified in Figure 6D. OFs were extended linearly with time, but interspersed with pauses, as observed for leading-strand only synthesis (Figure 3A). The burst rates of extension followed a Gaussian distribution (Figure 6H) with a mean of 550 ± 160 nt•s^{-1}, similar to the 510 ± 190 nt•s^{-1} observed for leading-strand-only synthesis (Figure 3B, top). Thus, the burst rate of polymerization is the same on both the leading and lagging strands; the polymerases function autonomously.

DISCUSSION

By observing replisome action on single molecules of DNA under conditions in which excess polymerases were removed, we have shown that the leading- and lagging-strand polymerases function autonomously. Surprisingly, leading-strand synthesis occurs in irregular bursts with spontaneous pauses independent of priming. During such pauses, helicase speed is reduced by about 80%, but when the leading-strand polymerase catches up with the helicase, the helicase resumes at full speed. Our data also show that the median processivity of lagging-strand synthesis at limiting primase is ~14 knt and confirms that the frequency of lagging-strand priming directly relates to primase concentration. Finally, we have shown that rates of replication on the leading and lagging strands are similar and that they are neither regulated by nor responsive to DNA priming nor primase.

Leading- and Lagging-Strand Polymerases Function Autonomously within a Single Complex

The classical view of DNA replication is uninterrupted leading-strand synthesis, with virtually infinite processivity, whereas a series of slower, rate-limiting steps is required to yield an OF. It has been assumed that lagging-strand synthesis must be faster to accommodate these slower steps. Our data suggest an alternative view in which polymerases within the replisome function autonomously. We find that replisome processivity changes little over a wide range of primase concentrations and that the leading-strand polymerase can function in the complete absence of primase. The polymerases share biochemical identity, and our data show that the single-turnover activity of leading- and lagging-strand polymerases is remarkably similar: burst rates and lengths on the leading and lagging strands are very closely matched. Lagging-strand processivity, revealed only at limiting primase concentration, is surprisingly high—much higher than physiological OF lengths—with a median of ~14 knt. In contrast, although leading-strand processivity is much higher, with a median of ~70 kb, the leading-strand polymerase displays an interesting propensity to pause every ~19 knt, which is curiously close to the processivity of the lagging-strand polymerase. Given that the burst rates are similar, this observation suggests that a rate-determining lifetime of the leading- and lagging-strand polymerase within the replisome is similar (Figures 3 and 6). This observation lends credence to the view that the two polymerases are autonomous.

Leading-Strand Replication Is Kinetically Discontinuous and Punctuated by Pauses and Rate Switching

Our data show that the leading-strand polymerase synthesizes DNA in kinetically discontinuous bursts, with pauses in between. However, the nascent 3′ terminus is localized near the helicase and available for elongation, so the resulting strand is chemically continuous. Priming the leading strand thus seems unnecessary for the short-term operation of the replisome, at least for the processivities we observe of tens to hundreds of kilobases. But for genomic DNA, however, a chemically discontinuous leading strand would be created at a lesion by priming downstream in the ssDNA between the polymerase and uncoupled helicase; in cells, the gaps could be filled and ligated later. Two independent sources of evidence support our view: (1) Okazaki's original work suggested that all the pulse label was in short fragments (Okazaki et al., 1967), and (2) leading-strand priming is required for the bypass of leading-strand lesions (Yeeles and Marians, 2011). In our rolling-circle assay, a single leading-strand discontinuity would terminate replication, as DnaB would unwind and run off the circular template. The single most likely cause of replication termination in our experiments is thus any long-lived pause or dissociation of the leading-strand polymerase lasting > 110 s (if unwinding of an 8.6 kb template occurs at ~80 bp•s^{-1}) or a chemical discontinuity on the leading-strand. Under most circumstances, disengagement or microscopic dissociation from the nascent 3′ terminus does not lead to termination because the polymerase is tethered to the helicase via τ, preventing macroscopic dissociation.

We note that previous single-molecule replication work was unable to deconvolve leading- and lagging-strand synthesis in reactions where the DNA was directly imaged: either no replication products were observed in the absence of primase (Tanner et al., 2011) or product detection required removal of SSB and hybridization of oligonucleotides to the leading strand to visualize molecule lengths at an end point (Georgescu et al., 2014; Yao et al., 2009). Moreover, the use of a minicircle template precluded the detection of pauses < ~1.3 s. Our larger rolling-circle substrate (~8.6 kb) permitted measurement of both the position and intensity of the template in real time, enabling us to both assess the role of primase in replication and correlate leading-strand synthesis pausing with template unwinding.

How do leading-strand pauses arise? The two most likely explanations are that the polymerase stalls at difficult-to-replicate DNA, which would be manifest as uncoupling of unwinding and replication, and that the helicase itself pauses at difficult-to-unwind secondary structure, which would manifest as a pause with no associated unwinding. However, a third possibility is that the polymerase randomly dissociates from either β or from DNA, as outlined above, either of which would require the reloading of β for continued synthesis. All these behaviors are observed in our data. We could identify no pattern to pausing,

as mapping the pause positions yielded no strong pause sites. Our data suggest that the leading-strand polymerase pauses every ~19 knt. However, the time resolution of our pause detection is ~3–4 s, and furthermore, any futile cycles of polymerization and unwinding without significant fork movement would not be detected. The pause durations (median = 13 s) were exponentially distributed—short pauses are under-represented—so our figure of ~19 knt for the kinetic burst size is likely to be an overestimate, and the average pause time is likely to be an overestimate. Taken together, our data show that leading-strand synthesis is unexpectedly dynamic, with kinetic pauses every few seconds. Below, we discuss the implication of these pauses for the interplay between unwinding and leading-strand synthesis.

The Replicative Helicase Incorporates a Fail-Safe Mechanism that Operates if Leading-Strand Synthesis Is Paused

We have shown that the speed of DnaB helicase unwinding is adjusted to match whether the leading-strand polymerase is actively elongating (high speed) or not (low speed). This finding concurs with our estimates of reduced helicase speed when interaction with the polymerase is disrupted (Kim et al., 1996). Our observations rationalize a long-observed disparity between the *E. coli* DnaB unwinding rate in isolation compared with that in the replisome (Kim et al., 1996; Ribeck et al., 2010; Yeeles and Marians, 2013) and support ensemble data obtained with the T7 replisome (Stano et al., 2005). Data from magnetic tweezer experiments revealed that the geometry and force imposed on DnaB may affect its speed (Ribeck et al., 2010), so perhaps the leading-strand polymerase, or its connection to the helicase via τ, may impose such a geometry or force. EM and crystallographic data imply that the N-terminal collar domain of DnaB adopts several conformational states, including "constricted" and "dilated," and it has been proposed that DnaC, primase, and τ may each effect the transitions between these states (Strycharska et al., 2013). Modulation of helicase speed, independent of primase, raises the possibility that helicase pausing results from slippage of the bipartite interaction between DnaB and the C-terminal domain of τ (Dallmann et al., 2000; Tougu et al., 1994), which binds core polymerase.

During a pause by DNA polymerase, where DnaB continues to unwind, the helicase does not necessarily physically disengage from the polymerase. The linkage connecting τ with core polymerase via DnaB is long and proline rich; with condensation of intervening ssDNA between helicase and polymerase by SSB (Bell et al., 2015), very long loops—up to several kilobases long—could be extruded between the two. This observation may partly explain why a deficiency in the SSB-χ interaction affects leading-strand polymerase stability (Marceau et al., 2011). Indeed, only 35% of polymerases (22 out of 62) did not find their way back to the helicase following a leading-strand pause. Our data suggest that leading-strand pauses of several minutes can be tolerated by the replisome and is entirely consistent with our previous observation of the spontaneous bypass of leading-strand lesions by replisomes (Yeeles and Marians, 2011). Under normal circumstances, priming would be biased toward the lagging-strand template based on the relative amounts of ssDNA present. Nevertheless, we can speculate that the leading-strand template might also be primed whenever the helicase moves sufficiently ahead of the polymerase, for instance, when a lesion is encountered on the leading-strand template (Yeeles and Marians, 2013).

In addition to pausing by the DNA polymerase while the helicase continues, we also observe pausing of the replication fork wherein DnaB stalls. The initiation of DnaB loading and movement is well regulated, but it would now appear that so, too, is its continued translocation during genome duplication. The most likely rationale for this plasticity is to reduce the rate of uncoupled unwinding of dsDNA, which would otherwise produce long tracts of SSB•ssDNA. DNA unwinding during replication therefore incorporates a fail-safe mechanism, akin to a "dead-man's switch," that prevents the production of long tracts of ssDNA should the leading-strand polymerase disengage or encounter a lesion.

Priming Frequency of the Lagging Strand Is Tuned to the Processivity of the Lagging-Strand Polymerase

Our data show that the frequency of lagging-strand priming far exceeds the inherent processivity of the polymerase. Priming more frequently than required may thus ensure that no large gaps are left in the genome. One outstanding question is therefore how such frequent OF synthesis can be accommodated without significantly slowing down the replication fork. It seems, from our data, that at maximal primase concentration, wherein OFs are synthesized every ~3 knt on average, the lagging-strand polymerase must dissociate from DNA and cycle to the next primer every ~6 s. Our data imply that the steps beginning from primer synthesis to the binding of core polymerase at a β-loaded 3′ primer terminus do not significantly slow replisome progression or otherwise occur on a timescale faster than the mean OF lifetime. Our observation here that both the leading- and lagging-stand polymerases can pause DNA synthesis every ~19 kb, in a primase- and priming-independent manner, offers a rate-limiting mechanism for matching the speeds of both polymerases.

One aspect not directly addressed by our data is the precise mechanism by which the polymerase cycles to the next OF. It is now generally accepted that most OFs are not replicated to a nick and that the lagging-strand polymerase dissociates prematurely, leaving behind a gap of tens of nucleotides. This phenomenon is often termed "signal release" (Wu et al., 1992b), and it has been suggested that the free 3′ primer terminus, not primase, acts as the trigger (Yuan and McHenry, 2014). Our data are most consistent with such a model.

A Stochastic View of Replisome Behavior

A central question in understanding replisome action is the mechanism by which the rates of leading- and lagging-strand synthesis are coordinated to ensure that unreplicated regions are not produced. Various solutions to this problem have been proposed. Many posit that for the additional enzymatic steps necessary for lagging-strand synthesis to be accommodated, the lagging-strand polymerase must synthesize DNA at a significantly faster rate than the leading-strand polymerase (Georgescu et al., 2014; Pandey et al., 2009; Selick et al., 1987). In

this manner, one would not expect the generation of significant gaps in the nascent lagging strand.

Our data indicate that such a deterministic model is unnecessary. The assumption that the rates of both polymerases are constant and are defined by their mean rates is flawed. We have shown that, whereas the mean rates of the leading- and lagging-strand polymerases are the same within error (510 ± 190 nt•s^{-1} versus 550 ± 160 nt•s^{-1}, Figures 3B and 6H), the rate profiles of individual polymerases are neither constant nor identical; they can randomly change to a new velocity within the Gaussian distribution. This intrinsic variability of rates, which reflects a molecular and switchable heterogeneity, had been demonstrated to be a manifestation of ergodic behavior in translocation rates of RecBCD enzyme (Liu et al., 2013). Our data, collected from fully assembled active replisomes, show that the rate of any polymerase can vary by 10-fold within the ensemble. This implies that, at any given time, the leading-strand polymerase can be synthesizing DNA at a rate faster than the lagging-strand polymerase, and vice versa. The sampling of wide distributions of rates and stochastic polymerase pausing obviates the need to impose differential rates for "coordinated" replication. This fluctuation in rates solves the coordination problem, with the leading-strand polymerase switching rates potentially every 15–20 kb after it pauses and the lagging-strand polymerase switching rates likely after each time that it initiates the synthesis of a new Okazaki fragment. Whereas transient gaps may form on any DNA template, they will be filled in over a short time range as the rates of synthesis vary. Such a statistical view of polymerase synthesis predicts a heterogeneous distribution of Okazaki fragment length on any particular DNA template, as we have observed here and as was observed using the bacteriophage T4 replication system (Chastain et al., 2000). Thus, we propose that the replisome solves the coordination paradox not by a deterministic regulated mechanism, but rather by stochastically sampling from a distribution of rates, a view that is consistent with existing data without invoking coordination.

STAR★METHODS

Detailed methods are provided in the online version of this paper and include the following:

- KEY RESOURCES TABLE
- CONTACT FOR REAGENT AND RESOURCE SHARING
- EXPERIMENTAL MODEL AND SUBJECT DETAILS
  - Source organism
- METHOD DETAILS
  - Microscopy
  - Coverslip preparation
  - Flow-cell assembly
  - Replication template
  - Recombinant proteins
  - Preparation of flow-cells for imaging
  - Rolling-circle replication reactions
  - End-point replication reactions
  - Live replication reactions
  - Okazaki fragment end-labeling and imaging
  - Preparation of λ DNA with an ssDNA gap
  - Length versus flow-rate for dsDNA and ssDNA•SSB
- QUANTIFICATION AND STATISTICAL ANALYSIS
  - Experimental resolution
  - Live imaging of leading-strand-only synthesis
  - Live imaging with primase
  - Lengths of replication end-products
  - Determination of Okazaki fragment terminus
- DATA AND SOFTWARE AVAILABILITY

SUPPLEMENTAL INFORMATION

Supplemental Information includes six figures, one table, and five movies and can be found with this article online at http://dx.doi.org/10.1016/j.cell.2017.05.041.

An audio PaperClip is available at http://dx.doi.org/10.1016/j.cell.2017.05.041#mmc7.

AUTHOR CONTRIBUTIONS

Conceptualization, Methodology, Writing – Review and Editing, Resources, Formal Analysis, J.E.G., K.J.M., and S.C.K.; Investigation, Software, Writing – Original Draft, Visualization, J.E.G.; Funding Acquisition, K.J.M., and S.C.K.; Project Administration, K.J.M. and S.C.K.

ACKNOWLEDGMENTS

We thank Soon Bahng (MSKCC) for purified proteins, Jody Plank for the template preparation protocols used in this work, James Berger (Johns Hopkins) for expression plasmids for mutant DnaG, and Michael Kohl (Oxford) for the basis of the edge-detection code used in this study. We thank all members of the S.C.K. group, especially Neville Gilhooly and Pham Minh Tuan, as well as David Sherratt (Oxford) and Joseph Yeeles (LMB, Cambridge), for their insightful comments on the work. These studies were supported by NIH grants GM34557 to K.J.M., GM064745 to S.C.K., and Cancer Center Core Support Grants NCI P30CA008748 to MSKCC and NCI P30CA093373 to UCD.

Received: November 9, 2016
Revised: March 29, 2017
Accepted: May 26, 2017
Published: June 15, 2017

REFERENCES

Alberts, B.M., Barry, J., Bedinger, P., Formosa, T., Jongeneel, C.V., and Kreuzer, K.N. (1983). Studies on DNA replication in the bacteriophage T4 in vitro system. Cold Spring Harb. Symp. Quant. Biol. *47*, 655–668.

Amitani, I., Liu, B., Dombrowski, C.C., Baskin, R.J., and Kowalczykowski, S.C. (2010). Watching individual proteins acting on single molecules of DNA. Methods Enzymol. *472*, 261–291.

Bell, J.C., Plank, J.L., Dombrowski, C.C., and Kowalczykowski, S.C. (2012). Direct imaging of RecA nucleation and growth on single molecules of SSB-coated ssDNA. Nature *491*, 274–278.

Bell, J.C., Liu, B., and Kowalczykowski, S.C. (2015). Imaging and energetics of single SSB-ssDNA molecules reveal intramolecular condensation and insight into RecOR function. eLife *4*, e08646.

Chastain, P.D., 2nd, Makhov, A.M., Nossal, N.G., and Griffith, J.D. (2000). Analysis of the Okazaki fragment distributions along single long DNAs replicated by the bacteriophage T4 proteins. Mol. Cell *6*, 803–814.

Corn, J.E., Pease, P.J., Hura, G.L., and Berger, J.M. (2005). Crosstalk between primase subunits can act to regulate primer synthesis in trans. Mol. Cell *20*, 391–401.

Dallmann, H.G., Kim, S., Pritchard, A.E., Marians, K.J., and McHenry, C.S. (2000). Characterization of the unique C terminus of the Escherichia coli tau

DnaX protein. Monomeric C-tau binds alpha AND DnaB and can partially replace tau in reconstituted replication forks. J. Biol. Chem. *275*, 15512–15519.

Dohrmann, P.R., Correa, R., Frisch, R.L., Rosenberg, S.M., and McHenry, C.S. (2016). The DNA polymerase III holoenzyme contains γ and is not a trimeric polymerase. Nucleic Acids Res. *44*, 1285–1297.

Duderstadt, K.E., Geertsema, H.J., Stratmann, S.A., Punter, C.M., Kulczyk, A.W., Richardson, C.C., and van Oijen, A.M. (2016). Simultaneous Real-Time Imaging of Leading and Lagging Strand Synthesis Reveals the Coordination Dynamics of Single Replisomes. Mol. Cell *64*, 1035–1047.

Forget, A.L., Dombrowski, C.C., Amitani, I., and Kowalczykowski, S.C. (2013). Exploring protein-DNA interactions in 3D using in situ construction, manipulation and visualization of individual DNA dumbbells with optical traps, microfluidics and fluorescence microscopy. Nat. Protoc. *8*, 525–538.

Geertsema, H.J., Kulczyk, A.W., Richardson, C.C., and van Oijen, A.M. (2014). Single-molecule studies of polymerase dynamics and stoichiometry at the bacteriophage T7 replication machinery. Proc. Natl. Acad. Sci. USA *111*, 4073–4078.

Georgescu, R.E., Yao, N., Indiani, C., Yurieva, O., and O'Donnell, M.E. (2014). Replisome mechanics: lagging strand events that influence speed and processivity. Nucleic Acids Res. *42*, 6497–6510.

Hiasa, H., and Marians, K.J. (1996). Two distinct modes of strand unlinking during theta-type DNA replication. J. Biol. Chem. *271*, 21529–21535.

Kim, S., Dallmann, H.G., McHenry, C.S., and Marians, K.J. (1996). Coupling of a replicative polymerase and helicase: a tau-DnaB interaction mediates rapid replication fork movement. Cell *84*, 643–650.

Langston, L.D., Indiani, C., and O'Donnell, M. (2009). Whither the replisome: emerging perspectives on the dynamic nature of the DNA replication machinery. Cell Cycle *8*, 2686–2691.

Lee, J.B., Hite, R.K., Hamdan, S.M., Xie, X.S., Richardson, C.C., and van Oijen, A.M. (2006). DNA primase acts as a molecular brake in DNA replication. Nature *439*, 621–624.

Liu, B., Baskin, R.J., and Kowalczykowski, S.C. (2013). DNA unwinding heterogeneity by RecBCD results from static molecules able to equilibrate. Nature *500*, 482–485.

Marceau, A.H., Bahng, S., Massoni, S.C., George, N.P., Sandler, S.J., Marians, K.J., and Keck, J.L. (2011). Structure of the SSB-DNA polymerase III interface and its role in DNA replication. EMBO J. *30*, 4236–4247.

Marians, K.J. (1995). Phi X174-type primosomal proteins: purification and assay. Methods Enzymol. *262*, 507–521.

Mok, M., and Marians, K.J. (1987). The Escherichia coli preprimosome and DNA B helicase can form replication forks that move at the same rate. J. Biol. Chem. *262*, 16644–16654.

Oakley, A.J., Loscha, K.V., Schaeffer, P.M., Liepinsh, E., Pintacuda, G., Wilce, M.C., Otting, G., and Dixon, N.E. (2005). Crystal and solution structures of the helicase-binding domain of Escherichia coli primase. J. Biol. Chem. *280*, 11495–11504.

Okazaki, R., Okazaki, T., Sakabe, K., and Sugimoto, K. (1967). Mechanism of DNA replication possible discontinuity of DNA chain growth. Jpn. J. Med. Sci. Biol. *20*, 255–260.

Pandey, M., Syed, S., Donmez, I., Patel, G., Ha, T., and Patel, S.S. (2009). Coordinating DNA replication by means of priming loop and differential synthesis rate. Nature *462*, 940–943.

Pham, T.M., Tan, K.W., Sakumura, Y., Okumura, K., Maki, H., and Akiyama, M.T. (2013). A single-molecule approach to DNA replication in Escherichia coli cells demonstrated that DNA polymerase III is a major determinant of fork speed. Mol. Microbiol. *90*, 584–596.

Pomerantz, A.K., Moerner, W.E., and Kool, E.T. (2008). Visualization of long human telomere mimics by single-molecule fluorescence imaging. J. Phys. Chem. B *112*, 13184–13187.

Ribeck, N., Kaplan, D.L., Bruck, I., and Saleh, O.A. (2010). DnaB helicase activity is modulated by DNA geometry and force. Biophys. J. *99*, 2170–2179.

Rymer, R.U. (2012). Studies on the Substrate Interactions of the Bacterial Primase. In Molecular & Cell Biology (University of California, Berkeley). http://escholarship.org/uc/item/3wr7f65j#page-1.

Schindelin, J., Arganda-Carreras, I., Frise, E., Kaynig, V., Longair, M., Pietzsch, T., Preibisch, S., Rueden, C., Saalfeld, S., Schmid, B., et al. (2012). Fiji: an open-source platform for biological-image analysis. Nat. Methods *9*, 676–682.

Selick, H.E., Barry, J., Cha, T.A., Munn, M., Nakanishi, M., Wong, M.L., and Alberts, B.M. (1987). Studies on the T4 bacteriophage DNA replication system. In Mechanisms of DNA Replication and Recombination, T. Kelly and R. McMacken, eds. (New York: Alan R. Liss), pp. 183–214.

Stano, N.M., Jeong, Y.J., Donmez, I., Tummalapalli, P., Levin, M.K., and Patel, S.S. (2005). DNA synthesis provides the driving force to accelerate DNA unwinding by a helicase. Nature *435*, 370–373.

Strycharska, M.S., Arias-Palomo, E., Lyubimov, A.Y., Erzberger, J.P., O'Shea, V.L., Bustamante, C.J., and Berger, J.M. (2013). Nucleotide and partner-protein control of bacterial replicative helicase structure and function. Mol. Cell *52*, 844–854.

Tanner, N.A., and van Oijen, A.M. (2009). Single-molecule observation of prokaryotic DNA replication. Methods Mol. Biol. *521*, 397–410.

Tanner, N.A., Loparo, J.J., Hamdan, S.M., Jergic, S., Dixon, N.E., and van Oijen, A.M. (2009). Real-time single-molecule observation of rolling-circle DNA replication. Nucleic Acids Res. *37*, e27.

Tanner, N.A., Tolun, G., Loparo, J.J., Jergic, S., Griffith, J.D., Dixon, N.E., and van Oijen, A.M. (2011). E. coli DNA replication in the absence of free β clamps. EMBO J. *30*, 1830–1840.

Thorpe, H.M., and Smith, M.C. (1998). In vitro site-specific integration of bacteriophage DNA catalyzed by a recombinase of the resolvase/invertase family. Proc. Natl. Acad. Sci. USA *95*, 5505–5510.

Tinevez, J.Y., Perry, N., Schindelin, J., Hoopes, G.M., Reynolds, G.D., Laplantine, E., Bednarek, S.Y., Shorte, S.L., and Eliceiri, K.W. (2017). TrackMate: An open and extensible platform for single-particle tracking. Methods *115*, 80–90.

Tougu, K., Peng, H., and Marians, K.J. (1994). Identification of a domain of Escherichia coli primase required for functional interaction with the DnaB helicase at the replication fork. J. Biol. Chem. *269*, 4675–4682.

Wu, C.A., Zechner, E.L., and Marians, K.J. (1992a). Coordinated leading- and lagging-strand synthesis at the Escherichia coli DNA replication fork. I. Multiple effectors act to modulate Okazaki fragment size. J. Biol. Chem. *267*, 4030–4044.

Wu, C.A., Zechner, E.L., Reems, J.A., McHenry, C.S., and Marians, K.J. (1992b). Coordinated leading- and lagging-strand synthesis at the Escherichia coli DNA replication fork. V. Primase action regulates the cycle of Okazaki fragment synthesis. J. Biol. Chem. *267*, 4074–4083.

Xu, L., and Marians, K.J. (2000). Purification and characterization of DnaC810, a primosomal protein capable of bypassing PriA function. J. Biol. Chem. *275*, 8196–8205.

Yao, N.Y., Georgescu, R.E., Finkelstein, J., and O'Donnell, M.E. (2009). Single-molecule analysis reveals that the lagging strand increases replisome processivity but slows replication fork progression. Proc. Natl. Acad. Sci. USA *106*, 13236–13241.

Yeeles, J.T., and Marians, K.J. (2011). The Escherichia coli replisome is inherently DNA damage tolerant. Science *334*, 235–238.

Yeeles, J.T., and Marians, K.J. (2013). Dynamics of leading-strand lesion skipping by the replisome. Mol. Cell *52*, 855–865.

Yuan, Q., and McHenry, C.S. (2014). Cycling of the E. coli lagging strand polymerase is triggered exclusively by the availability of a new primer at the replication fork. Nucleic Acids Res. *42*, 1747–1756.

STAR★METHODS

KEY RESOURCES TABLE

REAGENT or RESOURCE	SOURCE	IDENTIFIER
Antibodies		
Sheep anti-digoxigenin polyclonal F(ab) fragments	Roche	Cat# 11214667001, RRID: AB_514494
Bacterial and Virus Strains		
Escherichia coli BL21(DE3)	Novagen	Cat# 69450
Escherichia coli DH5α	Yale CGSC	Cat# 12384
Escherichia coli LE392	Promega	Cat# K9981
Escherichia coli XL2-Blue MRF′	Agilent Technologies	Cat# 200151
Chemicals, Peptides, and Recombinant Proteins		
Digoxigenin-11-dUTP, alkali-stable	Roche	Cat# 11558706910
Streptavidin	Promega	Cat# Z704A
Roche Blocking Reagent	Roche	Cat# 11096176001
Bovine Serum Albumin, fatty-acid free	Sigma	Cat# A8806
Acetone, CMOS-grade	JT Baker	Cat# JTP-9005-05
Methanol, CMOS-grade	JT Baker	Cat# JTP-9073-05
(3-aminopropyl)triethoxysilane (3-APTES)	Sigma	Cat# A3648
Biotin-PEG-NHS, MW 5000	Nanocs	Cat# PG2-BNNS-5k
mPEG-NHS, MW 5000	Nanocs	Cat# PG1-SC-5k
Hellmanex III	Sigma	Cat# Z805939
SYTOX Orange nucleic acid stain	Thermo Fisher	Cat# S11368
dNTPs (dATP, dGTP, dCTP, dTTP)	Jena Biosciences	Cat# NU-1009
NTPs (ATP, GTP, CTP, UTP)	Jena Biosciences	Cat# NU-1014
AMP-PNP	Jena Biosciences	Cat# NU-407
Alexa Fluor 488 NHS ester	Thermo Fisher	Cat# A20000
T7 DNA polymerase, unmodified	NEB	Cat# M0274
T4 DNA ligase	NEB	Cat# M0202
DNA Polymerase I (*Escherichia coli*)	NEB	Cat# M0209
Escherichia coli DNA ligase	NEB	Cat# M0205
DnaB	Marians, 1995	N/A
DnaC810	Xu and Marians, 2000	N/A
Pol III*	Marceau et al., 2011	N/A
DnaN (beta-clamp)	Hiasa and Marians, 1996	N/A
DnaG (primase; wild-type)	Marians, 1995	N/A
SSB	Bell et al., 2012	N/A
DnaG D269A	This study	N/A
DnaG D269Q	This study	N/A
Oligonucleotides		
Preparation of rolling-circle template: 80-mer, 5′ biotin-TEG- TTTTTTTTTTTTTTTTTTTTTTTTTTTTTTTTTTTTTTTTTTTTTTTTTTTTAATTCGT AATCATGGTCATAGCTGTTTCCT	This study	N/A
Preparation of λGap: 20-mer PCR primer, AGG ATC CAC AGG ACG GGT GT	Bell et al., 2012	N/A
Preparation of λGap: 20-mer PCR primer, ACT TTC ACC AGC GTT TCT GGG TG	Bell et al., 2012	N/A

(*Continued on next page*)

Continued

REAGENT or RESOURCE	SOURCE	IDENTIFIER
Mutagenesis of *dnaG*: D269A FW: 31-mer, CGAAGGCTATATGGCAGTGGTGGCGCTGGCG	This study	N/A
Mutagenesis of *dnaG*: D269A REV: 31-mer, CGCCAGCGCCACCACTGCCATATAGCCTTCG	This study	N/A
Mutagenesis of *dnaG*: D269Q FW: 31-mer, CGAAGGCTATATGCAGGTGGTGGCGCTGGCG	This study	N/A
Mutagenesis of *dnaG*: D269Q REV: 31-mer, CGCCAGCGCCACCACCTGCATATAGCCTTCG	This study	N/A
Preparation of dsDNA calibration standard: 12-mer GGGCGGCGACCT	This study	N/A
Recombinant DNA		
M13Ophrys	Bell et al., 2012	N/A
λKytos	Bell et al., 2012	N/A
pET28b(+)-*dnaG* (full-length; wild-type; TEV-cleavable His_6-tag)	James Berger (Johns Hopkins School of Medicine)	N/A
Software and Algorithms		
Adobe Illustrator (for laser cutter, Craft Robocutter patterns, preparation of figures)	Adobe Systems	Versions CS5, CS6
GraphPad Prism	GraphPad	Version 5.0b (Mac OS X)
Igor Pro	WaveMetrics	Version 6.x
Anaconda Python 2.7 distribution	Continuum Analytics	Python 2.7
Fiji ImageJ distribution	Schindelin et al., 2012	2015 December 22 build
Igor Pro code for end-product analysis (End-product and tract analyzer.ipf)	This study	https://github.com/jegra83/Cell_2017
Python code for extraction of data from TrackMate XML file (TrackMate XML to txt.py)	This study	https://github.com/jegra83/Cell_2017
Igor Pro code for measurement of product lengths from live imaging (Primase live imaging analyzer.ipf)	This study	https://github.com/jegra83/Cell_2017
ImageJ macro for extraction of template intensity from live leading-strand-only imaging (Intensity analyzer.ijm)	This study	https://github.com/jegra83/Cell_2017
Other		
PEEK tubing	Upchurch Scientific	Cat# 1532
PharMed tubing	Bio-Rad	Cat# 7318208
Double-sided tape	3M	Cat# 9437
Microscope slides, 75 × 25 mm	Fisher Scientific	Cat# 12-550-A3
Coverslip, FisherFinest #1, 22 mm square	Fisher Scientific	Cat# 12-548B
CO_2 laser cutter	Epilog	Mini 18
Epoxy Instant Mix 5 Minute	Loctite	Cat# 1365868

CONTACT FOR REAGENT AND RESOURCE SHARING

Further information and requests for resources and reagents, including custom analysis scripts, should be directed to and will be fulfilled by the Lead Contact, Stephen C. Kowalczykowski (sckowalczykowski@ucdavis.edu).

EXPERIMENTAL MODEL AND SUBJECT DETAILS

Source organism

All proteins used herein were purified from *Escherichia coli* K-12 strains (BL21(DE3) and DH5α) as described below. The replication template, M13Ophrys, was purified from *E. coli* XL2-MRF′ as described below. The ssDNA calibration standard, λGap, was generated from λKytos (Bell et al., 2012), which was purified from *E. coli* LE392.

METHOD DETAILS

Microscopy

Microscopy was performed on an Eclipse TE2000-U, inverted TIRF microscope (Nikon), using a CFI Plan Apo TIRF 100×, 1.49 numerical aperture, oil-immersed objective, and 488 nm and 561 nm lasers, as previously described (Amitani et al., 2010; Forget et al., 2013). Reactions were performed in single-use flow-channels, formed as described below. The replication template was an 8.6 kb Form II derivative of M13mp7 bearing a 5′ biotinylated dT_{50} flap, anchored to the surface via biotin-streptavidin linkage. The microscope was fitted with a CRISP autofocus system (ASI Instruments). The temperature of the flow-cell was maintained at 37°C throughout by a heated jacket fitted around the objective fed from a thermostatically controlled water bath. Images were captured using a DU-897E iXon EMCCD camera (Andor, 100 ms exposure), with an effective pixel size of 162.9 nm at 100 × magnification.

Coverslip preparation

Coverslips (FisherFinest #1, 22 mm square) were subjected to a 30 min piranha clean (3 parts H_2SO_4 (conc.) to 1 part 30% (v/v) H_2O_2), followed by submerging four times in MilliQ water and 30 min methanolic KOH (~1.3 M) treatment with sonication. After submerging a further four times in MilliQ water, coverslips were submerged twice for 10 min in CMOS-grade acetone (JT Baker), the second time with sonication. Coverslips were functionalized with primary amine groups using (3-aminopropyltriethoxy)silane (Sigma; 2% (v/v) in acetone) for 5 min with agitation, submerged an additional four times in MilliQ water, and baked at 120°C for ~30 min to cure the silane. After cooling, coverslips were PEGylated by applying a viscous mixture of PEG and biotin-PEG to one side of the coverslip; a second coverslip was placed on top of the first to make a sandwich, and a third non-functionalized coverslip placed along the edge of the sandwich to aid prising apart of the PEGylated coverslips. The outside faces of the sandwich were scribed to aid identification of the PEGylated side (Tanner and van Oijen, 2009). PEGylation was at room temperature in the dark for ~3 hr, in 100 mM $NaHCO_3$ (pH 8.4) with a mix of 1:50 biotin-PEG-NHS ester to mPEG-NHS ester (Nanocs); total final PEG concentration ~15% (w/v). Following 4-5 rinses using a jet of MilliQ water, coverslips were dried under a stream of N_2 gas and stored in the dark, under vacuum, at room temperature, for up to two weeks before use.

Flow-cell assembly

Each flow-cell consisted of three independent single-use channels, each of which had its own inlet and outlet port. Holes of ~1 mm diameter, 10 mm apart, were etched in standard 25 × 75 mm uncoated glass microscope slides with an Epilog CO_2 laser cutter followed by drilling (Forget et al., 2013). Slides were cleaned by immersion in 2% (v/v) Hellmanex III solution overnight followed by sonication for 30 min in methanolic KOH (~1.3 M). Inlet and outlet ports, made of ~1 cm long PEEK tubing (Upchurch Scientific, #1532) were sharpened using a rotary sander, inserted into the cut holes of the microscope slides, and glued in place using a five-minute epoxy (Loctite). Once the epoxy had set, the sharpened ends of the PEEK tubing were trimmed with a razor blade. Three 2.5 × 12.5 mm channels were cut using a Craft Robocutter (GraphTec) in 19 × 19 mm squares of double-sided tape (3M #9437; thickness 51 μm), and flow-cells were assembled with double-sided tape sandwiched between slide and coverslip. The resulting flow-channels were 2.5 × 12.5 × 0.051 mm (~1.6 μl). For live reactions, the channels were cut with dimensions of 1.25 × 12.5 × 0.051 mm, resulting in a flow-cell volume of ~0.8 μl.

Replication template

An 8.6-kb derivative of M13mp7 circular ssDNA bearing the *attB* integration site for ϕC31 integrase (M13Ophrys) and an ampicillin resistance gene was used as template (Bell et al., 2012). M13Ophrys was purified as follows. First, a phage stock was prepared by transforming the double-stranded form of the vector into DH5α and plating on LB agar containing 100 μg/ml ampicillin at 37°C. The following day, 25 mL of 'GB' medium (LB containing 8.5 mM KH_2PO_4, 36 mM K_2HPO_4, and 0.5% (v/v) glycerol), containing 100 μg/ml ampicillin was inoculated with a single colony from the agar plate and grown overnight at 37°C with shaking at 200 rpm. *E. coli* cells were pelleted by centrifugation at 4,000 x *g* for 30 min and the supernatant containing phage retained. Phage was precipitated by the addition of 0.5 M NaCl, 5% (w/v) PEG-8000 (final concentrations) to the supernatant on ice for 2 hr, pelleted by centrifugation at 4,000 x *g* for 30 min, and resuspended in ice-cold buffer containing 25 mM Tris-HCl (pH 7.5 at 4°C), 10 mM $Mg(OAc)_2$, 100 mM NaCl, and 50% (v/v) glycerol. The phage stock was stored at –20°C until use.

To generate the circular ssDNA form of M13Ophrys, *E. coli* XL2 Blue-MRF′ was streaked on LB agar containing 34 μg/ml chloramphenicol and grown overnight at 37°C. In the morning, a single colony was inoculated into 3 mL of GB medium (above) containing 34 μg/ml chloramphenicol in a test tube, and incubated at 37°C with shaking at 200 rpm. After ~4 hr, once the culture had become turbid, 100 μl of the phage stock generated above was added and growth continued at 37°C for ~2 hr. 100 mL of GB medium (above) containing 34 μg/ml chloramphenicol and 50 μg/ml ampicillin was inoculated with 100 μl of the phage-infected culture, and growth continued overnight at 37°C. 50 mL of the culture was pelleted the following morning by centrifugation at 4,000 x *g*; the supernatant containing phage was retained and pelleted as described above.

Circular M13 ssDNA was purified using a QIAGEN maxiprep kit, using buffers supplied by the manufacturer, and with the protocol modified as follows: phage pellets were resuspended in 10 mL Buffer P1; 10 mL Buffer P2 was added, mixed gently, and incubated for 5 min to lyse the phage. 10 mL Buffer P3 was added to neutralize the sample and precipitate the protein, SDS and DNA for 10 min, followed by clarification by centrifugation at 4,000 x *g* for 30 min. The clarified supernatant was further filtered through

a Kimwipe using a 50 mL plastic syringe. A single QIAGEN tip-500 column was equilibrated with 15 mL Buffer QBT. The clarified lysate was added to the column and allowed to enter the resin bed. The column was washed with 5 mL of ssDNA wash buffer (50 mM MOPS (pH 7.0), 900 mM NaCl, 15% (v/v) isopropanol), then twice further, each time with 30 mL ssDNA wash buffer. Circular DNA was eluted with 20 mL of 50 mM MOPS (pH 7.0), 1 M NaCl, 4 M deionized urea, 15% isopropanol; precipitated with the addition of 14 mL of isopropanol; and pelleted by centrifugation at 4,000 x *g* for 60 min. The DNA pellet was washed twice with 10 mL of room temperature 70% (v/v) EtOH, and dissolved overnight at 4°C in 100 μl TE buffer (10 mM Tris-Cl (pH 8.0 at 4°C), 1 mM EDTA). The purity and integrity of the substrate was verified by 0.8% alkaline and neutral agarose gel electrophoresis.

To generate the rolling-circle template, oligonucleotide oJEG38 (5′-TTTTTTTTTTTTTTTTTTTTTTTTTTTTTTTTTTTTTTTTTTTT TTTTTT AATTCGTAATCATGGTCATAGCTGTTTCCT-3′), bearing a 5′ biotin-triethylene glycol moiety and 50-nt flap, was synthesized (Integrated DNA Technologies) and purified by urea-PAGE and avidin-agarose. The oligo was annealed to M13Ophrys via 30 nt of complementarity and extended using T7 DNA polymerase (NEB) in the presence of 200 μM dNTPs to create a biotin-tailed Form II template. Extension of the primer to generate a nicked circle was monitored by 0.8% alkaline and neutral agarose gel electrophoresis of the products. Products were purified by two rounds of phenol-chloroform extraction followed by ethanol precipitation.

Recombinant proteins

Untagged *E. coli* DnaB, DnaC810, wild-type primase (DnaG), β (DnaN), SSB and Pol III* were purified as described (Hiasa and Marians, 1996; Marceau et al., 2011; Marians, 1995; Xu and Marians, 2000). Mutant *E. coli* primases (D269A, D269Q) bearing N-terminal TEV-cleavable His_6-tags, were purified as follows. Primase was overexpressed in *E. coli* BL21(DE3) by adding 1 mM IPTG to the culture at OD_{600} ~0.8 for 4 hr at 37°C. Cells were lysed by passage twice through a French press (12,000 psi) in 50 mM Tris-Cl (pH 7.5 at 4°C), 10% (v/v) glycerol, 150 mM NaCl, 20 mM EDTA, 1 mM DTT, 1 mM PMSF, and 20 mM spermidine, and debris removed by centrifugation at 44,000 × *g* for 20 min. The pH of the lysate was adjusted to 8.0 using solid Tris base. Following lysis, genomic DNA was precipitated and removed by dropwise addition of a 10% (v/v) solution of Polymin P (pH 8.0) to 0.04% (v/v) and centrifugation at 30,000 × *g* for 20 min. Protein in the resulting supernatant was precipitated with 50% saturated ammonium sulfate and centrifuged as above. The pellet was dissolved in ~50 mL of 50 mM Tris-Cl (pH 7.5 at 4°C), 10% (v/v) glycerol, 500 mM NaCl, 10 mM imidazole and dialyzed for 2 hr against the same buffer in a volume of 4 L. The dialysate was applied to a 5 mL HisTrap column (GE) and protein eluted in a gradient of 0-500 mM imidazole over ten column volumes. Pooled fractions (~30 mg) were diluted to 50 mL by 50 mM Tris-Cl (pH 7.5 at 4°C), 10% (v/v) glycerol, 10 mM NaCl; 1.4 mg His-tagged TEV protease was added for cleavage overnight at 4°C. The cleaved protein was reapplied to the HisTrap column as above, and untagged primase collected in the flow-through. Cleaved mutant primase was dialyzed ~2 hr against 50 mM Tris-Cl (pH 7.5 at 4°C), 10% (v/v) glycerol, 10 mM NaCl, 1 mM EDTA, 5 mM DTT (Buffer A) and diluted ~3-fold for application to a 5 mL HiTrap heparin column equilibrated with the same buffer. The flow-through was reapplied twice to the column. Protein was eluted in a 10-600 mM NaCl gradient over ten column volumes; DnaG eluted at ~125 mM NaCl. Approximately 9 mg total protein was obtained. The protein was dialyzed against Buffer A, applied to a MonoQ (10/10) column equilibrated with Buffer A, and eluted with a 10-500 mM NaCl gradient over ten column volumes. The pure fractions (6.6 mg protein) were dialyzed against 50 mM Tris-Cl (pH 7.5 at 4°C), 50 mM NaCl, 1 mM EDTA, 5 mM DTT, 38% (v/v) glycerol, and snap-frozen in liquid nitrogen for storage at –80°C. The mutant primase preparations contained no detectable ssDNA or dsDNA nuclease activity.

Preparation of flow-cells for imaging

Single-molecule imaging buffer (SMB) contained: 50 mM HEPES-KOH (pH 8.0), 10 mM magnesium acetate, 25 mM KCl, 15% (w/v) sucrose. DTT (50 mM) was added in powdered form fresh to the buffer on the day of use; the buffer was passed through a 0.22-μm syringe-driven filter and degassed for ~4 hr. Each flow-channel was prepared immediately before use by pipetting in the following sequence: 100 μL SMB; 100 μL SMB containing 0.1 mg/ml streptavidin (Promega; ~21°C, 2 min); 100 μL SMB. The flow-cell was then connected to the injection system using ~5 mm pieces of PharMed tubing (Bio-Rad) to connect the PEEK tubing to the inlet and outlet ports. All surfaces, including connecting tubing, were blocked against nonspecific binding by flowing 1 mL of SMB containing 1% (w/v) blocking reagent (Roche; cat. 11096176001) through the flow-cell at 10 $ml \cdot h^{-1}$. Blocking reagent was removed by flowing another 1 mL of SMB through the system at 10 $ml \cdot h^{-1}$. The replication template was adsorbed to the surface by introducing SMB containing ~10 pM (molecules) replication template and 75 nM SYTOX Orange into the flow-cell. The density of DNA molecules could be adjusted by a 10-fold concentration of template (from 10 to ~100 pM) and time (from 1 to ~10 min) without buffer flow; for end-point reactions, a lower density of molecules was preferred so that molecules would not overlap when elongated by replication.

Rolling-circle replication reactions

The overall experimental scheme was to first attach an 8.6 kb template via a 5′ biotinylated tail to the surface (‘anchor’). Next, idling replisomes were formed by introducing DnaB, DnaC810, Pol III*, β, three out of the four dNTPs, and all rNTPs. Following a wash to remove unbound proteins, replication was initiated by adding dTTP and flow-stretching the DNA. SSB, β and primase were present in flow.

Specifically, following adsorption of DNA to the surface and the removal of excess DNA once the desired density of template had been achieved, the syringe, lines and flow-cell were equilibrated with wash buffer (‘WB’; SMB (as above) plus 1 mM ATP, 200 μM each CTP, GTP and UTP, 40 μM each dATP, dCTP and dGTP [no dTTP], and 75 nM SYTOX Orange). On the day of use, replication

proteins were diluted to fifteen times the required concentration from stock in a buffer containing 50 mM Tris-Cl (pH 7.5), 10 mM beta-mercaptoethanol, 1 mM EDTA, 100 mM NaCl, 500 μg/ml BSA, and 20% (v/v) glycerol (protein diluent, 'PD'). Reactions were performed in two stages: a pre-incubation "bind" mix (50 μl) contained 60 nM DnaB (as hexamer), 380 nM DnaC810, 20 nM Pol III*, 30 nM DnaN (β, as dimer), and 10 μg/ml BSA in WB (with additionally one-fifth equivalent of PD). Primase was not added to the pre-incubation mix. Flow-cells were washed with 25 μL WB (~90 s, 1,000 μl•h^{-1}), after which reactions were initiated with a "start" mix (60 μL for end-point reactions; 150 μL for live reactions), containing 320 nM primase, 250 nM SSB (as tetramer), 30 nM DnaN (β, as dimer), 40 μM dTTP (in addition to the other three dNTPs), and 10 μg/ml BSA in WB (with additionally one-fifth equivalent of PD). Pre-incubation, wash, and start mix were injected in-line into the flow-cell using a system of injection loops driven by a syringe pump. Flow was maintained at 1,000 μl•h^{-1} during the pre-incubation and wash stages, and was altered as appropriate during the reaction (below). The volume required to initiate the reaction was determined empirically by injecting fluorescent dye into the flow-cell. For dropout and titration experiments, the concentration of protein was varied as appropriate (see main text).

End-point replication reactions

For end-point reactions, flow was reduced to 100 μl•h^{-1} without constant laser illumination; reactions were only periodically illuminated with the 561 nm laser to check the progress of the reaction. At 10 min, reactions were quenched by injection of 50 μL SMB containing 75 nM SYTOX Orange, 1 mM AMP-PNP, 40 μM each dATP, dCTP and dGTP and ddTTP, at 4,000 μl•h^{-1}. The flow-cell and lines were washed and equilibrated with SMB lacking magnesium acetate, plus 15 nM SYTOX Orange ("end-point imaging buffer"). The removal of Mg^{2+} ion (i) prevented further DNA synthesis; (ii) improved the signal-to-noise ratio of fluorescence intensity detection, as the affinity of SYTOX Orange stain for dsDNA is higher in the absence of divalent cation; and (iii) relieved the compaction of ssDNA•SSB, improving the resolution of regions of any possible gaps on the lagging strand (Figure S1F). Where necessary (main text), the flow was shut off for ≥ 20 s and the molecules allowed to recoil. Between 20 and 50 frames at 100 ms exposure were recorded. All end-products were extended at a flow-rate of 4,000 μl•h^{-1} for visualization, and an additional 20-50 frames recorded. Between 40 and 200 fields were recorded for each flow-channel by imaging in a serpentine path to avoid field duplication. For each dataset, a 'flat' image was recorded by defocusing 1-2 μm from the surface into bulk solution and taking an average of 8-10 points in the flow-channel. Each image for that dataset was then normalized by dividing the intensity values by the 'flat' image values.

Live replication reactions

Reactions were performed as described above, except in a flow-cell of half the width (~0.8 μL volume) to permit double the linear flow-rate for a given volumetric flow-rate. Upon starting the reaction with a defined volume of the 'start' mix, the flow-rate was adjusted to 1,250 μl•h^{-1}, the equivalent of 2,500 μl•h^{-1} in the end-point reactions above. Movies were recorded at a low level of laser exposure, determined empirically not to cause appreciable photocleavage to λ DNA, at a frame rate of 7.4 Hz.

Okazaki fragment end-labeling and imaging

Reactions were performed exactly as for the end-point experiments above, except that at 10 min, 50 μL of SMB containing 1 M NaCl was injected into the flow-cell to remove bound proteins and SYTOX Orange. The high-salt buffer was immediately followed by 400 μL WB at 4,000 μl•h^{-1} without stopping the flow. Replication products were pulse-labeled by injecting 50 μL of a mix comprising: 30 mM Tris-Cl (pH 8.0 at 25°C), 10 mM magnesium acetate, 10 μg/ml BSA, 40 μM each of dATP, dCTP and dGTP, 20 μM digoxygenin-11-dUTP (alkali-stable, Roche), 26 μM NAD^+, 3.3 U DNA Pol I (wild-type, full-length, NEB), 3.3 U *E. coli* DNA ligase (NEB), and 250 nM SSB (as tetramer), at a flow-rate of 500 μl•h^{-1} for 5 min. At 5 min, a further 50 μL SMB + 1 M NaCl was introduced to remove bound Pol I and ligase, immediately followed by a further wash of 400 μL WB at 4,000 μl•h^{-1}, again without stopping flow. Sheep polyclonal anti-digoxigenin F(ab) fragments (Roche), labeled with Alexa Fluor 488 NHS ester (ThermoFisher Scientific) with an average of 3.6 dyes per molecule, were injected into the flow-cell in end-point imaging buffer, at ~300 nM molecules; 250 nM SSB (tetramer) was also included to replenish any removed during the high-salt wash. Excess F(ab) fragments and SSB were washed out of the flow-cell and products imaged using the same buffer. There was no appreciable nonspecific binding of labeled F(ab) fragments to the surface. Alexa Fluor 488 and SYTOX Orange signals were imaged on two halves of the EMCCD using a Dual-View apparatus (Optical Insights) and bandpass filters specific to each dye (Chroma), illuminating the sample alternately with the 488 nm and 561 nm lasers. DNA was imaged under a flow-rate of 8,000 μl•h^{-1}.

The 5′ and 3′ locations of each OF were inferred from the patterns of 3′ terminus labeling and the positions of gaps (see Figure 5A). To estimate the labeling efficiency, we determined the proportion of resolvable ssDNA•SSB gaps which had a detectable focus at their right-hand edge, *i.e.*, the 3′ terminus of the right-hand OF (Figure 5A), which acted as an internal control (Table S1).

Preparation of λ DNA with an ssDNA gap

Bacteriophage M13mp7 ssDNA containing the *attB* recognition site was used to generate a 500 bp dsDNA fragment containing the ϕC31 *attB* at its center by PCR using the Phusion High Fidelity PCR Master Mix from NEB. The dsDNA product was heat denatured, and then annealed to the M13mp7 ssDNA derivative. The gapped λ DNA was generated by site-specific recombination between λ*Kytos* dsDNA and the annealed M13mp7 ssDNA containing the *attB* recognition site (M13Ophrys), using ϕC31 integrase. The ϕC31 integrase was purified from plasmid pHS62 (Thorpe and Smith, 1998).

Length versus flow-rate for dsDNA and ssDNA·SSB

To prepare dsDNA as a calibration standard, a 3′-biotinylated oligonucleotide (5′-GGGCGGCGACCT-3′) was ligated to λ DNA (N^6-methyladenine-free; NEB) using T4 DNA ligase. For the ssDNA•SSB length calibrations, λKytos DNA bearing an internal 8,155 nt gap ("λGap") was prepared as described (Bell et al., 2012) and the same biotinylated oligonucleotide ligated. DNA was introduced into a flow-cell as described above and imaged in SMB containing 75 nM SYTOX Orange, 1 mM ATP, 200 μM each CTP, GTP and UTP, 40 μM dNTPs and 250 nM SSB (as tetramer, for the gapped substrate only); then the buffer in the flow-cell was exchanged into SMB containing 15 nM SYTOX Orange, but lacking magnesium acetate and lacking SSB. The first condition mimics the replication reaction conditions, and the second the end-point imaging conditions. The calibrations were performed sequentially to mimic the experiments described above. DNA was imaged at flow-rates between 100 and 9,000 $\mu l \cdot h^{-1}$, and twenty frames recorded and averaged. Molecules were analyzed as described below. The central gap in λGap could not be resolved below a flow-rate of 2,000 $\mu l \cdot h^{-1}$ in the Mg^{2+}-free buffer, and 2,500 $\mu l \cdot h^{-1}$ in the Mg^{2+}-containing buffer. Data were binned and fitted to single Gaussians to determine the mean length (±standard deviation; Figure S1).

QUANTIFICATION AND STATISTICAL ANALYSIS

Statistical details of individual experiments, including numbers of observations and replicates, dispersion and precision measures, are as described in the manuscript text, figure legends, and the figures themselves. Specific treatments of data are as described in detail below.

Experimental resolution

Given the maximum wavelength of fluorescence emission for SYTOX Orange is ~570 nm, our experiments have a nominal resolution of ~285 nm (given the calibrations above and in Figure S1, ~0.9 kb dsDNA, or 2.4 knt ssDNA•SSB under end-point imaging conditions; ~1.0 kb dsDNA and 3.2 kb ssDNA•SSB under live imaging conditions). All molecule lengths were converted from a pixel length to base-pairs (for dsDNA tracts) or nucleotides (for ssDNA•SSB tracts) based on the calibrations described above. The time resolution of the experiments is also outlined below.

Live imaging of leading-strand-only synthesis

For live reactions, images were averaged using a sliding window average of five frames, and the stack size reduced 5-fold, resulting in a time resolution of ~680 ms. A rolling-ball filter of 50 pixels was used to subtract background from the image stacks. For reactions lacking primase, template positions were tracked automatically using the Fiji TrackMate plugin for ImageJ (Schindelin et al., 2012; Tinevez et al., 2017). The code locates the centers of spots within individual frames of an image stack, then solves a linear assignment problem to link the positions of spots from successive frames together. Spot centers were located using a Laplacian of Gaussian (LoG) detector, with an estimated blob diameter of 8 pixels, applying a median filter and threshold to reduce false positives. Typically, ~200-300 spots were found per frame. Because the particles track left to right under flow, a large *y*-direction penalty was applied during frame-to-frame linking. Track segment gap closing was permitted with a typical maximum distance of 10 pixels and gap of 3 frames, to account for frames in which spots were not detected owing to fluctuations in flow.

This process typically generated up to a thousand tracks, most of which were exceedingly short (several pixels long), resulting either from template that does not move (*i.e.*, did not have a loaded replisome), or which moved only a short distance. Therefore, a further filter was applied to remove low-quality tracks that had < 50 spots (with a frame interval of ~0.7 s), and moved 5 pixels (~9 knt). This process reduced the number of tracks to ~100-150, of which only ~50 were uninterrupted by another molecule. Tracks were also manually inspected to ensure that the linking algorithm did not aberrantly link the trajectories of two adjacent spots together. All data were manually inspected for mistracking artifacts such as the proximity of a non-moving or paused template molecule, by using both the overlay of the spot positions on the data and the shape of the resultant tracks.

Track displacements were determined using a Python script to extract the track coordinates and calculate the template displacements from the XML output of TrackMate. The displacement in pixels was converted to a nucleotide displacement value using the calibrations determined above. Pause positions and burst velocities were determined by fitting the traces piecewise to three-segment lines by a non-linear least-squares method (GraphPad Prism), constraining the velocity of the middle segment to zero.

Template intensities were determined using a custom-written ImageJ macro, using a circle of radius 5 pixels drawn at the fitted template position in each frame. Background intensities were subtracted from the data using a circle of 5-pixel radius drawn above or below the midpoint of the template track. The intensity in each track was normalized, assuming the maximum intensity would correspond to the template size (~8.6 kb). Unwinding velocities were determined by linear fits to the normalized intensity data, using the pause points determined above to define the periods of unwinding. Only unwinding rates from active replisomes were determined, although data were pooled from terminal unwinding events and unwinding events that occurred midway through synthesis.

Processivity values were determined independently of the TrackMate method by projecting the maximum intensity per frame over the image stack to generate a composite image showing the tracking of the template over time. The length of the track at the reaction end-point could thus be measured using the end-point procedure described below.

Replication fork rates were determined from a single-segment linear fit, using the initiation and termination points of the fork as start and end points of the line.

Live imaging with primase

Frames were averaged using a seven-frame sliding window, resulting in a time resolution of ~1 s. The LoG tracking method above could not sufficiently distinguish between template and the tail of duplex DNA behind the replication fork. We therefore used an edge-detection method using a custom-written routine in Igor Pro (Wavemetrics). The intensity values of a 1D line profile (of constant co-ordinates across the image stack) were taken across the molecule of interest, incorporating a ~10-20 pixel flanking region on each side of the molecule for calculation of an internal signal-to-noise standard. A low-pass frequency filter was applied to reduce noise and the first-order differential of the data calculated to locate the intensity change-points. The background signal was then used to calculate a detection threshold, using the background plus an arbitrary number of standard deviations above the mean (between 3 and 6, depending on the inherent signal-to-noise of the data). Positive (dsDNA tract start) and negative (dsDNA tract end) peaks in the first-order differential exceeding the threshold were located using Igor Pro's level-detection function. This method resulted in the occasional detection of spurious edges, which could be eliminated by changing the number of standard deviations used for the thresholding (at the expense of sensitivity), and by using a sliding-window algorithm to eliminate outliers. Replication fork rates were thus determined by a linear fit to the data from initiation to termination, ignoring any pauses during the elongation phase. All pixel values were converted to a leading-strand length value, taking into account the ssDNA•SSB or dsDNA content of the product at a particular time-point. The same edge detection method was used for the special case of limiting primase (1 nM in flow) as per Figures 6 and S6 and Movie S5. Growth of the Okazaki fragment, as well as progression of the fork, was isolated and monitored, fitting the OF data piecewise to three-segment lines as necessary, as described above. Molecules whose paths coincided with stationary template were rejected.

Lengths of replication end-products

End-point images, acquired in the absence of Mg^{2+} ion as described above in End-point replication reactions, consisted of stacks of ~20-50 images of each field with the flow on or off, as necessary ('flow-on' or 'no-flow', respectively). The signal-to-noise of these images was inherently higher than for the live imaging data owing to the absence of Mg^{2+}, so further denoising was unnecessary. Image stacks (with or without flow) were median-averaged, then normalized by dividing by the 'flat' image, also described above. For molecules where 'no-flow' data were acquired, a composite image of the 'flow-on' and 'no-flow' background-corrected images was created by false-coloring the grayscale data, with the images overlaid but treated as separate channels (Figure S2). Molecules were analyzed by using a custom-written routine in Igor Pro (Wavemetrics). The routine entails drawing a 1D line profile manually across the molecule of interest; the start- and end-points of dsDNA tracts are then located by taking the first-order differential of the 1D profile, and finding the crossing-points above a threshold, which was defined as at least three standard deviations above the mean of an equivalent background 1D profile. For molecules that were subjected to the flow-cycling analysis to locate anchor points, the anchor was assigned as the peak of the fluorescence along the same 1D profile in the 'no-flow' channel of the composite image. The uncertainty introduced by this method is outlined with a dsDNA control in Figure S2C. We define 'tracts' as any contiguous pieces of SYTOX Orange-stained dsDNA without a resolvable gap (> 1.2 knt), but a 'tract' at higher primase concentrations might consist of multiple OFs (Figure 4A).

Determination of Okazaki fragment terminus

Background-corrected images (using a 'flat' image; see End-point replication reactions above) from Alexa Fluor 488-labeled 3′ ends and SYTOX Orange-stained dsDNA were registered and overlaid to make a composite image, using at least ten fiducial markers present in both channels across a number of fields. The ''Landmark Correspondences'' plugin of Fiji was used for registration (Schindelin et al., 2012); rigid body rotation and translation of the SYTOX Orange image was allowed. The intensity profile of a molecule of interest was taken from a line profile in the SYTOX Orange channel (dsDNA); dsDNA tract and gap positions were determined as above. The same line coordinates were used to generate the Alexa Fluor 488 intensity profile as the SYTOX Orange channel; Okazaki fragment 3′ termini were located on the line by fitting an arbitrary number of peaks to the intensity profile using Igor Pro's multi-peak fitting package, with a constant linear baseline. The mean and standard deviation of the background were determined from a line drawn outside any molecules of interest; only peaks that were at least three standard deviations above the background mean were considered. Our method also labels the circular template, which is ignored in this analysis (Figure 5A).

To determine the precise locations of 3′ termini in replication products, a 1D line profile was taken across each molecule based on its SYTOX Orange fluorescence intensity. The 1D line profile of Alexa Fluor 488 intensity was then fitted to a series of Gaussian peaks; Figure S5 shows fits for data at 320 nM (**A**), 10 nM (**B**) and 1 nM (**C**) primase; the flow-cycling method above was only necessary at 2 nM primase and below. We then used the positions of the foci to calculate mean OF lengths and priming distances as a function of primase concentration.

DATA AND SOFTWARE AVAILABILITY

Four custom scripts used in this study have been made available at: https://github.com/jegra83/Cell_2017.

End-product flow and tract analyzer.ipf is an Igor Pro (WaveMetrics) macro both for measuring the lengths of replication end-products and finding the positions and lengths of dsDNA tracts from SYTOX Orange fluorescence micrographs, as defined in Figure 4A. The macro detects the edges of tracts by taking the first derivative of a 1-dimensional (1D) line profile drawn across a molecule of

interest. Anchor points are determined, where appropriate, from images where the flow was turned off. The user positions cursors on an image flanking the molecule of interest; tract positions are shown interactively on a 1D fluorescent line profile, so false positives can be identified. Positions of the starts and ends of ssDNA•SSB and dsDNA tracts recorded within a text file for subsequent calculations, using the calibrations of Figure S1; the total length of a particular molecule is then merely the sum of the individual ssDNA and dsDNA tract lengths for that molecule.

TrackMate XML to txt.py is a Python 2.7 script that converts the XML output of TrackMate into CSV format. TrackMate was used to track the position of the rolling-circle template for live imaging without primase. The script outputs the frame number, *x* and *y* positions of the template, and the calculated displacement of the template, relative to the first frame in which the template was detected, using the ssDNA•SSB extension versus flow calibrations of Figure S1.

Primase live imaging analyzer.ipf is an Igor Pro macro that automates the location of ssDNA•SSB and dsDNA tracts in time-series data. It is functionally similar to End-product flow and tract analyzer.ipf described above. Like the macro described above, a 1D line profile is taken across a molecule of interest, except that given the lower signal-to-noise in time-series data compared to static images, the profiles at each time-point were filtered using a low-pass filter, and smoothed using a boxcar function. This macro was used for live imaging in the presence of primase both in Figure 1D–1G (320 nM primase) and Figure 6D–6H (1 nM primase).

Intensity analyzer.ijm is an ImageJ macro used for determining the intensity with respect to time of the rolling-circle template from live imaging data in the absence of primase. It takes the *xy* coordinates of each molecule from time-series data (the output of TrackMate XML to txt.py described above) and returns a time-series of the integrated intensity of a circle of radius 5 pixels drawn at the exact location of the template. Background fluorescence was determined separately by integrating the intensity of another circle of 5-pixel radius, in a fixed location in the same field, close to the trajectory of the molecule of interest, but across which the template did not move during the imaging.

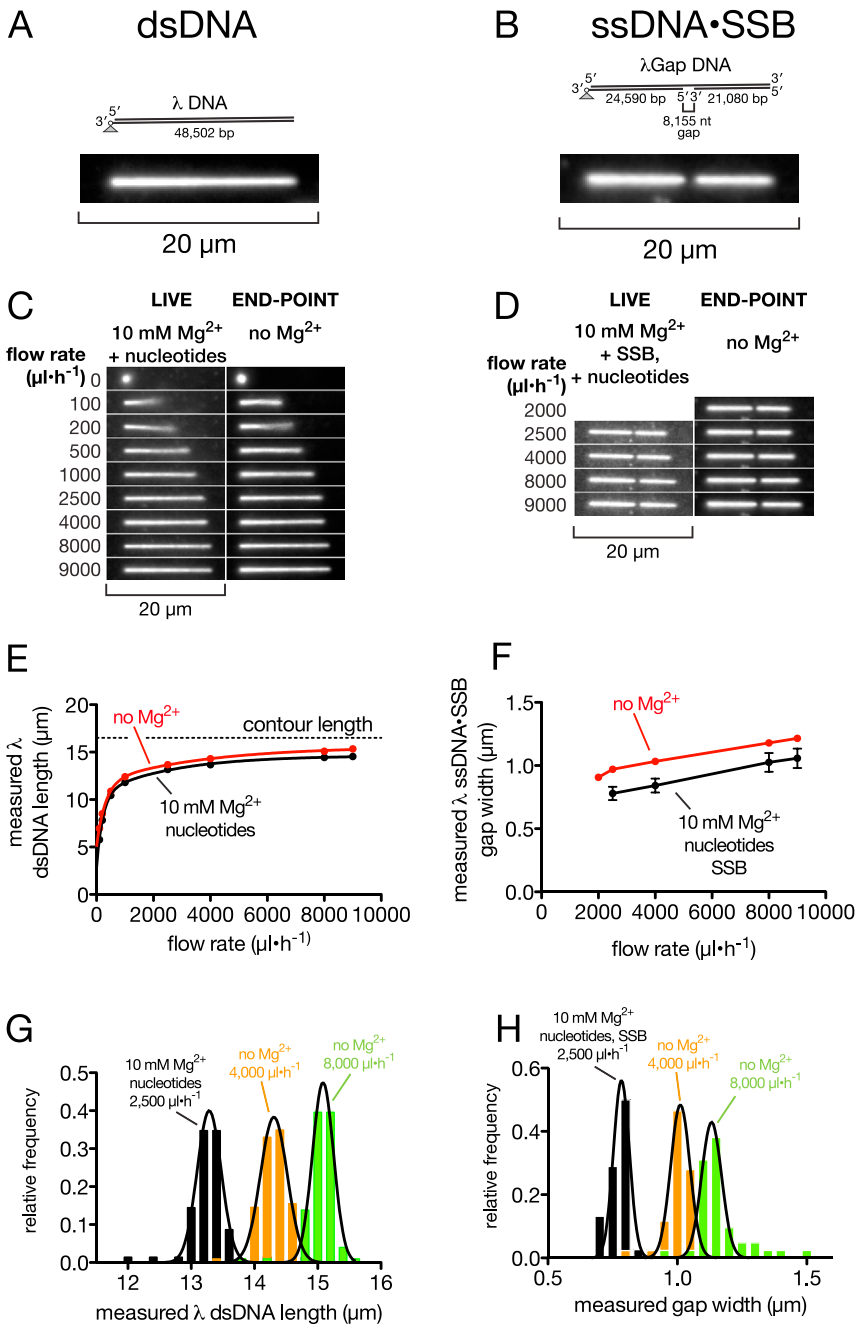

Figure S1. Calibration of dsDNA and ssDNA·SSB Extension against Volumetric Flow-Rate under Reaction Conditions and Visualization Conditions, Related to Figure 1

(A) Cartoon of control DNA (λ dsDNA; 48,502 bp) used to calibrate flow-cells for duplex DNA extension at a given flow-rate. Molecules were anchored to the surface via single biotin-streptavidin linkage at one end. A representative molecule is shown under the highest flow-rate (9,000 μl•h^{-1}) without Mg^{2+} ion present; bracket width 20 μm.

(B) Cartoon of control DNA (λGap) used to calibrate flow-cells for SSB•ssDNA extension at a given flow-rate. The control DNA is a derivative of λgt11 bearing a defined 8,155 nt ssDNA gap and flanking regions of ~25 kb and ~21 kb dsDNA proximal and distal to the anchor, respectively (Bell et al., 2012). Molecules were anchored to the surface as per (A). A representative molecule is shown under the highest flow-rate (9,000 μl•h^{-1}) without Mg^{2+} ion present; bracket width 20 μm.

(C) Snapshots of λ dsDNA molecules at given volumetric flow-rates, under live imaging conditions ("LIVE"); or end-product visualization conditions ("END-POINT"). The calibrations were performed sequentially in the presented order. No proteins were included in the flow.

(D) Snapshots of λGap molecules at given volumetric flow-rates, under live imaging conditions ("10 mM Mg^{2+} SSB & nucleotides"); or end-product visualization conditions ("no Mg^{2+}"). The calibrations were performed sequentially in the presented order. SSB (250 nM tetramer) was present in flow under the 10 mM Mg^{2+}

(legend continued on next page)

condition and not under the Mg^{2+}-free condition. Data for the 10 mM Mg^{2+} condition below 2,500 μl•h^{-1} are not shown because the gap could not be adequately resolved.

(E) Calibration of duplex dsDNA extension versus volumetric flow-rate under live or end-product visualization conditions. Data are the mean of ten molecules per condition; error bars (±SEM) are smaller than the markers. Data are fit to a double-exponential, $y = y_0 + A_1(1 - e^{-k_1 x}) + A_2(1 - e^{-k_2 x})$. Fit parameters: 10 mM Mg^{2+} + nucleotides: y_0 = 2.8 ± 0.48 μm, A_1 = 7.8 ± 0.42 μm, k_1 = 0.0045 ± 0.00065, A_2 = 4.1 ± 0.35 μm, k_2 = 0.00038 ± 7.1 × 10^{-5}; no Mg^{2+} (and no nucleotides): y_0 = 5.0 ± 0.33 μm, A_1 = 3.9 ± 0.35 μm, k_1 = 0.00028 ± 7.9 × 10^{-5}, A_2 = 6.7 ± 0.40 μm, k_2 = 0.0033 ± 0.00051 (all ± SE of fit; R^2 > 0.98 for both fits).

(F) Calibration of ssDNA•SSB extension versus volumetric flow-rate. Data are the mean of 14 molecules ("LIVE") or 4 molecules ("END-POINT") per condition; error bars (SEM) are smaller than the markers for the no-Mg^{2+} condition. Data ≥ 2,500 μl•h^{-1} were fit by linear regression (R^2: 10 mM Mg^{2+}, nucleotides + SSB: 0.999; no Mg^{2+}, 0.98).

(G and H) Calibration of dsDNA and ssDNA•SSB extension under three experimental conditions: histograms of dsDNA and ssDNA lengths are shown under live imaging (black); and end-product visualization conditions (orange: standard end-product visualization; green: Okazaki fragment labeling experiments). Buffer conditions were as indicated. The higher flow rate slightly reduced off-axis Brownian motion, permitting better resolution of anti-digoxigenin foci (Figure 5), at the expense of an increased breakage rate of products due to combination of shear flow and photocleavage. Number of observations: (G): black: 69; orange: 103; green: 101; (H): black: 38; orange: 43; green: 42. Molecules were recorded in at least three different positions in at least two different flow-cells. Histograms were fit to Gaussian distributions, with means: G (dsDNA): black: 13.3 ± 0.19 μm; orange: 14.3 ± 0.21 μm; green: 15.1 ± 0.17 μm; H (ssDNA•SSB): black: 0.78 ± 0.03 μm; orange: 1.01 ± 0.04 μm; green: 1.13 ± 0.04 μm (±SD of distribution; R^2 for all fits > 0.95).

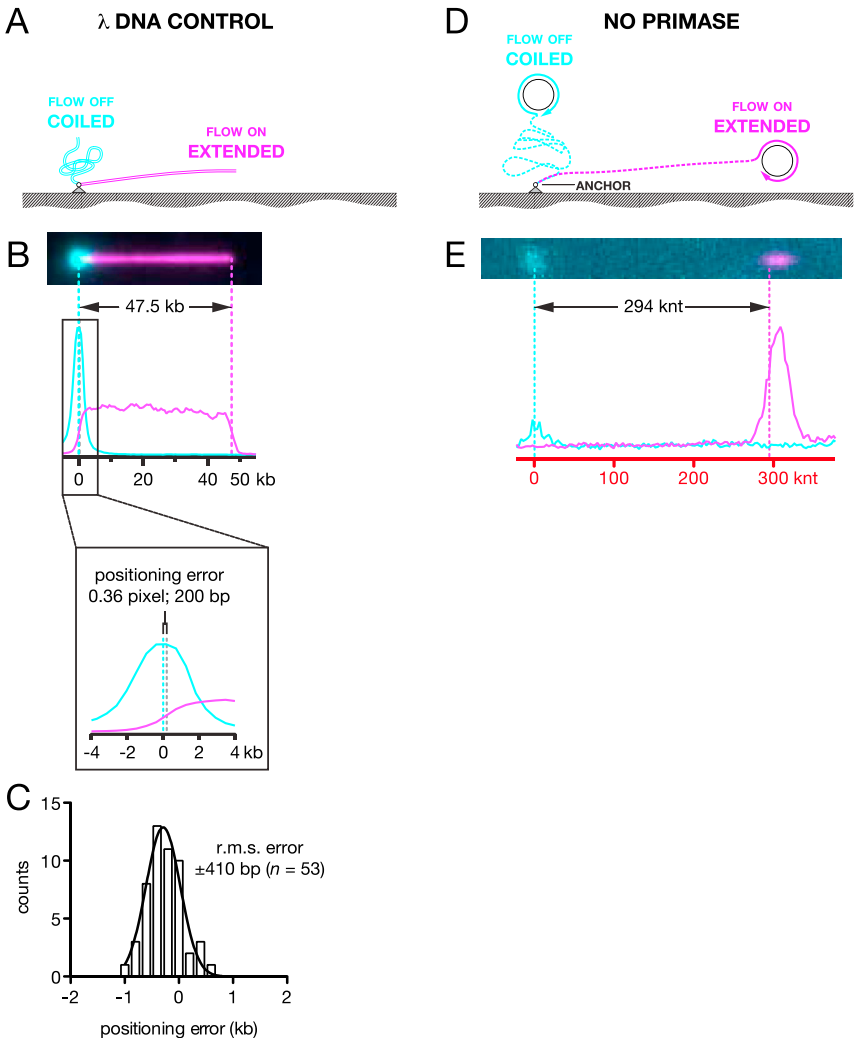

Figure S2. Determination of the Anchor-Point of Leading-Strand Replication Products, Related to Figure 2

(A) Validation of the method used to determine anchor points of replication products using a λ dsDNA control. Cartoon showing flow-cycling method used to determine anchor points of λ dsDNA, with coiled molecules in cyan and flow-extended molecules in magenta, as per Figure 2B-2G.

(B) False-colored, representative molecule showing SYTOX Orange-stained λ dsDNA. The positioning error of the anchor-point is determined from the difference in position between the half-maximum of the intensity of the λ dsDNA at the anchored end (gray dashed line) and the anchor point as determined by shutting off the flow (cyan dashed line).

(C) Positional accuracy of the anchor points determined by the flow-cycling method, calculated from 53 λ dsDNA molecules that were subjected to the analysis of (B). The root-mean-squared variation of the determined compared with the actual anchor point was ± 410 bp, ~0.5% the mean length of a replication product from a 10 min reaction.

(D) Cartoon showing flow-cycling method used to determine anchor points in reactions that are expected to produce only ssDNA, as per (A).

(E) False-colored, representative molecule showing SYTOX Orange-stained replication product in a reaction lacking primase. Anchor point was determined by taking the mean position of the coiled molecule by recording the average of multiple frames with the flow turned off, and the product length determined by the distance from anchor to the half-maximum intensity of the circular template of the product when extended. Plot below shows fluorescence intensity profile of a line drawn across the axis of extension of the molecule.

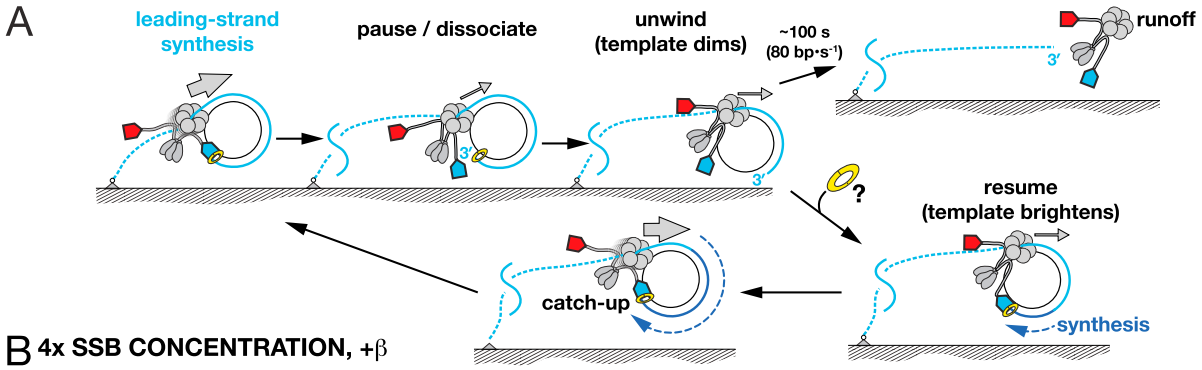

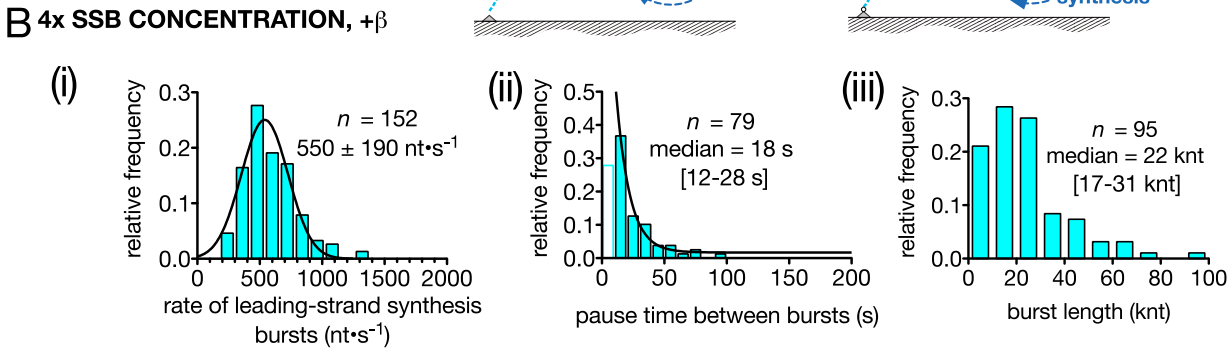

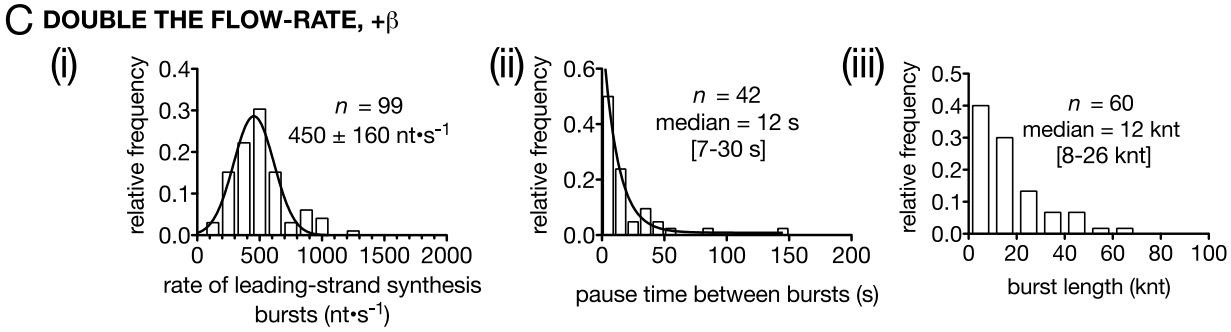

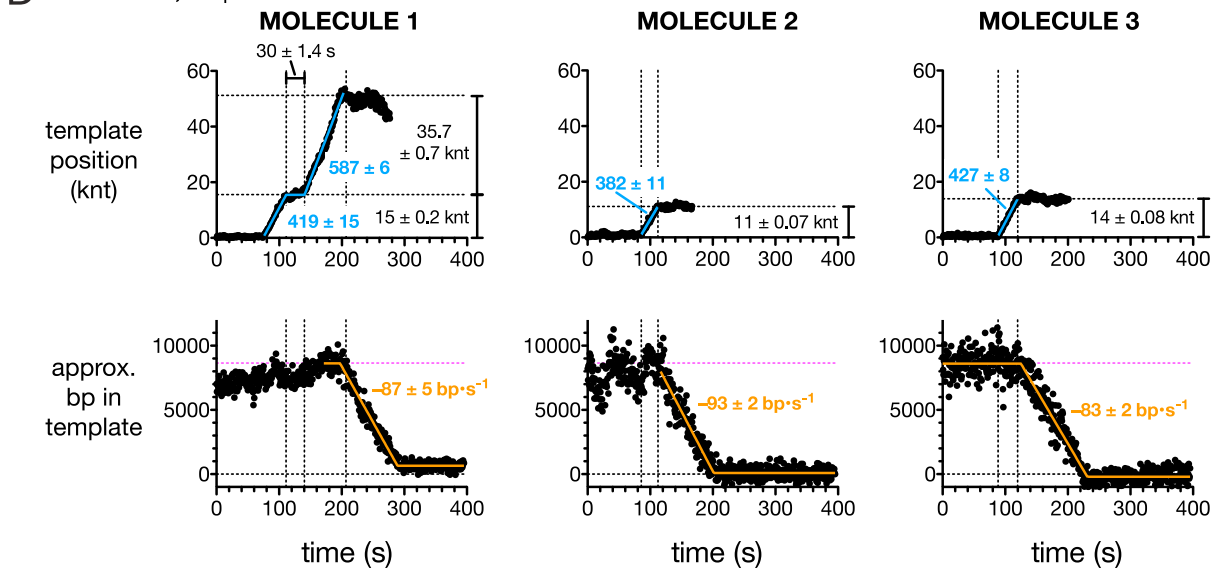

(legend on next page)

Figure S3. Effects of the Absence of β, Increased SSB Concentration, and Increased Flow on Leading-Strand Replication, Related to Figure 3

(A) Cartoon showing the possible intermediates resulting from a transient pause by the leading-strand polymerase. The steps of polymerase pausing or dissociation, slowed uncoupled DNA unwinding by the helicase, and either helicase runoff or synthesis resumption and polymerase "catch-up" are shown. The cartoon shows the polymerase dissociating from the 3′ end of the leading strand, which happens in some cases, but in other cases the polymerase will remain bound to the 3′ end during the stall period.

(B and C) Effect on (i) rates of leading-strand synthesis bursts, (ii) pause times, and (iii) burst lengths under conditions of (B) at quadruple the SSB concentration, or (C) double the flow-rate. To address whether pausing is caused by transient condensation of ssDNA by SSB, we performed control experiments in which we increased the SSB concentration in flow to 1 μM tetramer, and doubled the flow-rate. Histograms showing distributions from single control experiments, with the stated numbers of observations. Rates were fit to Gaussians (±SD), and pause times fit to single exponentials, ignoring the unshaded bin in B, ii; burst lengths exhibited a variety of distributions, so we report here the medians of the populations. Neither treatment had a significant effect on the burst velocity or on the pause duration, although increasing SSB concentration slightly increased the kinetic burst rate, to 550 ± 190 $nt \cdot s^{-1}$. However, the length of synthesis bursts was slightly reduced at the higher flow-rate, which we attribute to the increased force on the replisome. Thus, it is unlikely that pauses in synthesis can be attributed to simple sequestration of secondary structure.

(D) The absence of β from flow reduces replisome processivity and leads to terminal unwinding. Data from three representative molecules (molecules 1, 2, and 3) are shown, with template position (top) and estimated base-pairs remaining in the template (bottom). These molecules are also shown in Movie S4. Blue figures represent burst rates (in $nt \cdot s^{-1}$) for the replisome fitted to three-segment lines (blue lines; ± SE of fit); orange figures represent template DNA unwinding rates (in $bp \cdot s^{-1}$) fitted to two- or three-segment lines (the latter, where complex behavior was not seen before the terminal unwinding event; orange lines; ± SE of fit). Magenta dotted lines in lower panels indicate the maximum number of base-pairs in the template (8,644 bp).

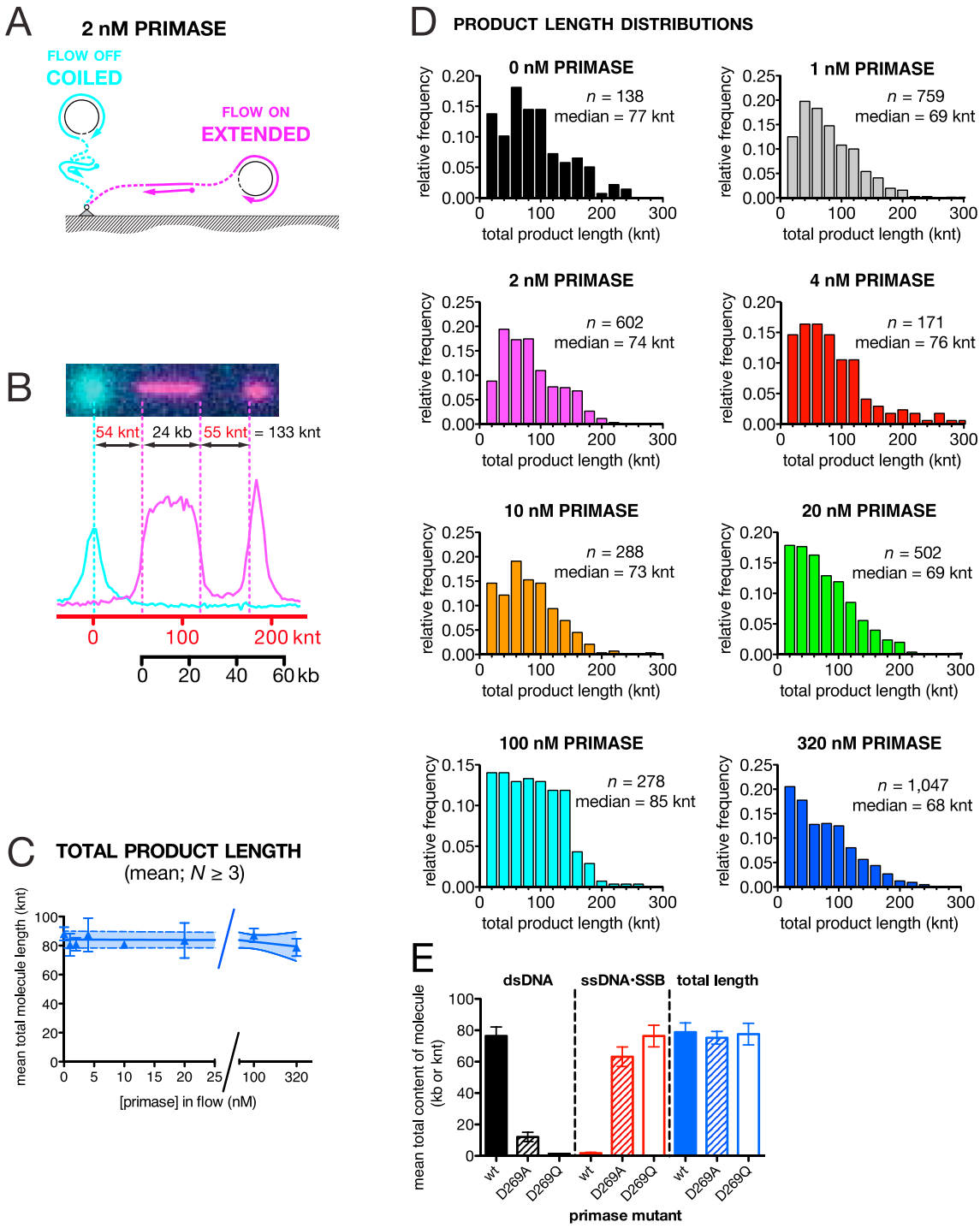

Figure S4. The Length of the Leading Strand in Replication Products Is Independent of Primase Concentration, Related to Figure 4

(A) Cartoon showing the method used to determine anchor points of replication products at low primase concentration: flow was turned off, and replication products allowed to extend from their anchors (cyan); products were also imaged with the flow on (magenta).

(B) Representative product at 2 nM primase with the intensity profile of a 1D line drawn through the molecule shown underneath. Scale bars show lengths of SSB•ssDNA (red) and dsDNA (black), for these flow conditions.

(C) Graph showing total molecule (leading-strand, SSB•ssDNA plus dsDNA) length as a function of primase. Data are the means of means (±SEM) from at least three experiments. Blue line is a linear fit to the data, with blue shading indicating 95% confidence bands of fit.

(D) Histograms showing total product lengths as primase is increased from 0 to 320 nM. Data pooled from at least three experiments, with the number of observations and the population median stated on the histograms.

(legend continued on next page)

(E) Total dsDNA (black), total ssDNA (red), and total product length (blue) for replication products, with reactions performed in the presence of 320 nM of wild-type primase (solid bars), or two catalytic mutants (D269A; shaded bars, D269Q; open bars). Data shown are the means (±SEM) from three replicates. Median dsDNA content, 7.4 kb (IQR, 2.0-16.0 kb) and none detected for D269A and D269Q, respectively; median total lengths: D269A, 70 knt; D269Q, 72 knt (IQR, 42-100 knt and 43-101 knt, respectively). Replicates, N = 3; molecules: D269A, n = 195; D269Q, n = 173.

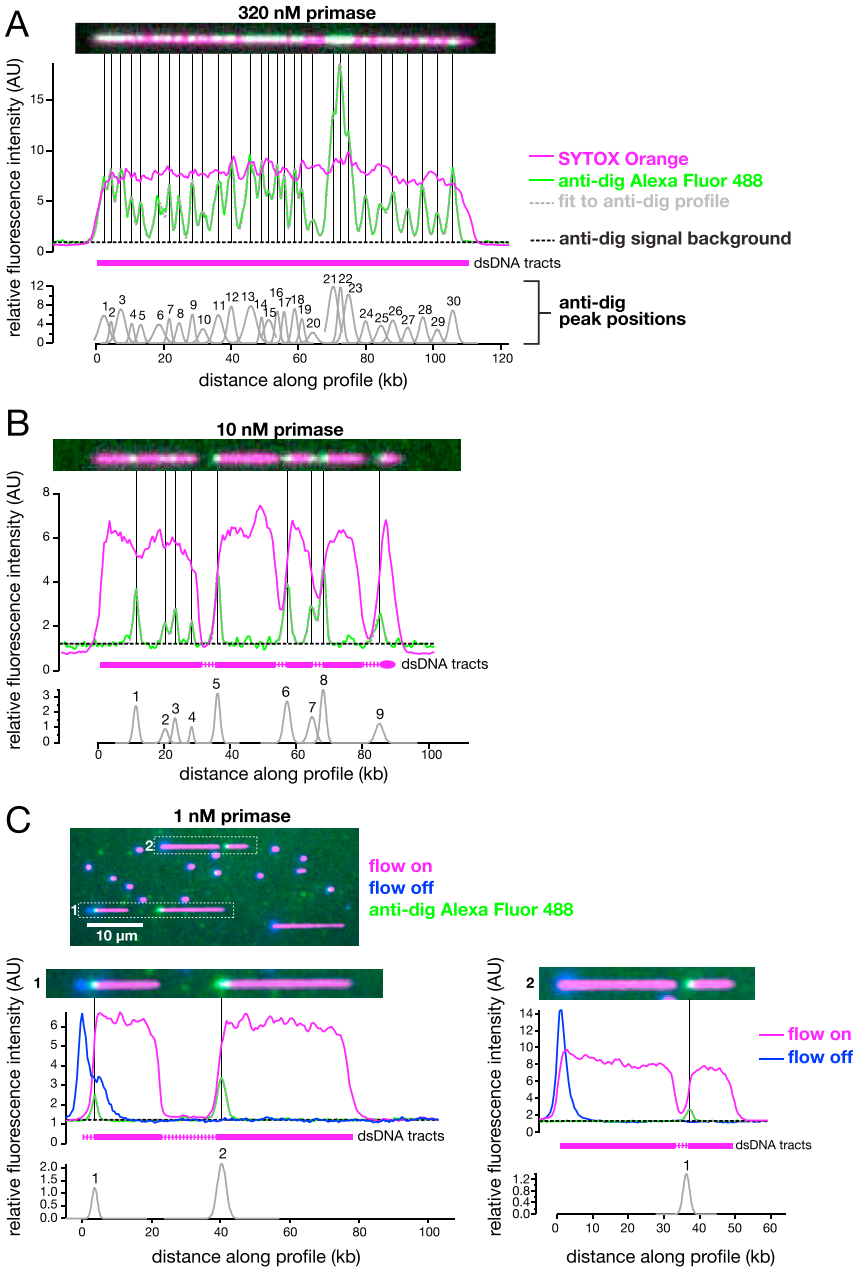

Figure S5. Method for the Location of 3′ Termini of Okazaki Fragments, Related to Figure 5

(A–C) Reaction end-products were treated with Pol I and ligase in the presence of digoxigenin-labeled dUTP, yielding 3′-labeled OFs. The dsDNA is stained with SYTOX Orange and OF ends stained with labeled anti-digoxigenin. Magenta, dsDNA tracts; green, OF 3′ termini. Representative molecules and analysis at (A) 320 nM primase, (B) 10 nM primase, and (C) 1 nM primase (two molecules shown for 1 nM primase). Raw image data are shown (top), with SYTOX Orange stain (dsDNA, magenta), 3′ ends (anti-digoxigenin Alexa Fluor 488, green), and anchor points (blue, 1 nM primase only, determined as per Figures S4A and S4B). Fluorescence intensity profiles taken along a line are shown underneath; the middle panel shows the raw intensity traces with multi-peak Gaussian fitting of the anti-digoxigenin foci to determine the centroids of the foci (vertical lines). Bottom panels show expanded detail of the fitted widths, heights and positions of the individual peaks.

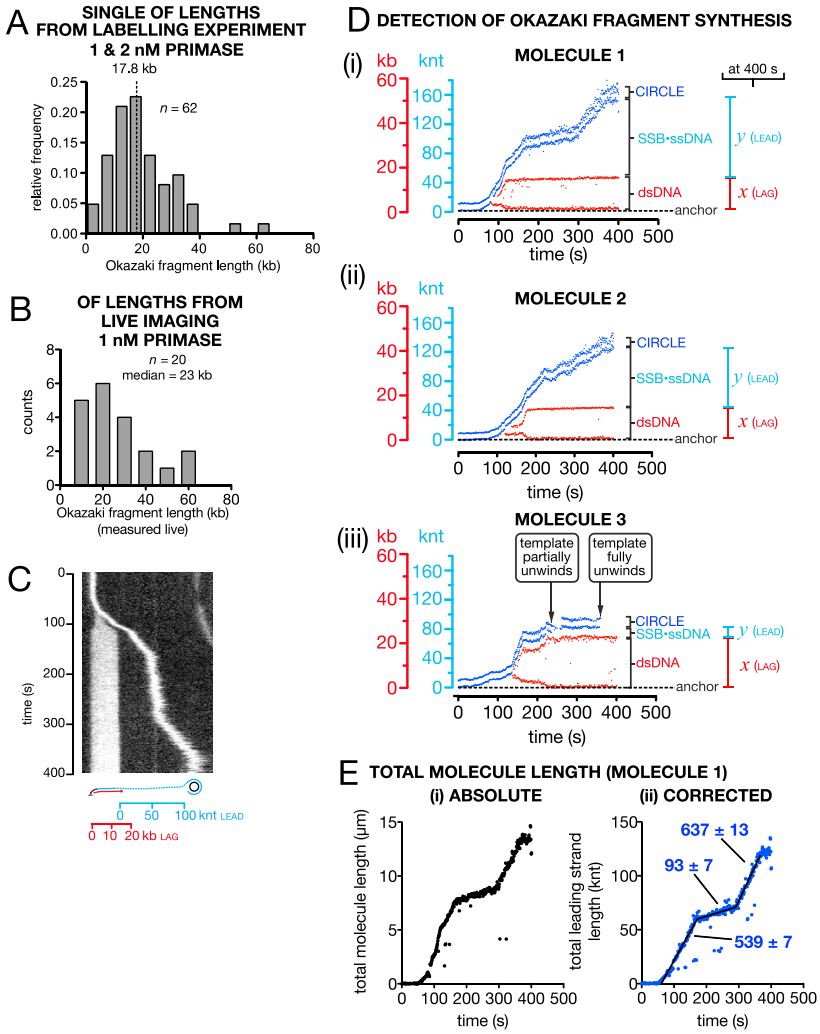

Figure S6. Okazaki Fragment Synthesis Rates and Lengths, Determined from End-Point and Live Imaging Experiments, Related to Figure 6

(A) Histogram showing distribution of Okazaki fragment lengths determined directly from 3′ end-labeling experiments (Figures 5 and S5). Data (N = 3) pooled from experiments at 1 nM (N = 2) and 2 nM primase (N = 1), with 62 observations.

(B) OF lengths determined from live imaging experiments, where products were continuously held under flow; N = 5.

(C) Representative kymograph of molecule 1 (as identified in Figure 6D-G) undergoing periods of leading- and lagging-strand synthesis in the presence of 1 nM primase and SYTOX Orange dsDNA stain. Cartoon shows an interpretation of fluorescent signal at 400 s.

(D) Example traces for the three molecules identified in Figure 6D (i, ii and iii), showing detection of edges of Okazaki fragments (red) and the circular template (dark blue), and thereby the definition of Okazaki fragment length (red, *x*), leading-strand length (blue, *y*) and the anchor point (dotted black line). Molecule 3 exhibits two phases of template unwinding at approx. 225 and 350 s, the latter of which is terminal.

(E) (i) Plot of the absolute length of molecule 1 as a function of time, as judged by the distance from the anchor-point to the nearest edge of the template. (ii) Plot of the length of molecule 1 converted to base-pairs, taking into account the relative compaction of dsDNA versus ssDNA•SSB.